



INSTITUTO
UNIVERSITÁRIO
DE LISBOA

Design of All-Metal Antennas for 5G and Satellite Applications

Fábio Martinho Cardoso

Master Degree in,
Telecommunications and Computer Engineering

Supervisor:
PhD Sérgio de Almeida Matos, Assistant Professor,
Iscte - IUL

Co-supervisor:
PhD Jorge Manuel Lopes Leal Rodrigues da Costa, Full Professor,
Iscte - IUL

November, 2021



TECNOLOGIAS
E ARQUITETURA

Department of Information Science and Technology

Design of All-Metal Antennas for 5G and Satellite Applications

Fábio Martinho Cardoso

Master Degree in,
Telecommunications and Computer Engineering

Supervisor:
PhD Sérgio de Almeida Matos, Assistant Professor,
Iscte - IUL

Co-supervisor:
PhD Jorge Manuel Lopes Leal Rodrigues da Costa, Full Professor,
Iscte - IUL

November, 2021

Preface

The work presented in this dissertation was carried out in IT BRANCH – ISCTE-IUL (Lisbon, Portugal), during the period October 2020 – October 2021, under the supervision of Prof. Dr. Sérgio A. Matos and Prof. Dr. Jorge R. Costa. This thesis was partially supported by Fundação para a Ciência e Tecnologia (FCT) under projects PTDC/EEI-TEL/30323/2017 (“ADAM3D”) and UIDB/50008/2020.

Part of the results of this thesis was **accepted** and **presented** as a communication in the *Special Session – Antennas, Beamsteering and Radio Imaging*, in CONFTELE2021:

F. Cardoso, S. A. Matos, J. R. Costa and C. A. Fernandes, "Design of an All-Metal Broadband Rotman Lens for Satellite Communications at K/K_a-Band," 2021 Telecoms Conference (ConfTELE), Leiria, Portugal (Online), February 2021, pp. 1-4, doi: 10.1109/ConfTELE50222.2021.9435483.

The final results of this thesis were submitted as a communication, to the conference EuCAP2022:

F. Cardoso, S. A. Matos, J. R. Costa, C. A. Fernandes, J. Felício and N. J.G. Fonseca “Design of a Rotman Lens Operating in the Full K/K_a Band Using Ridge Waveguide Technology” 16th European Conference on Antennas and Propagation (EuCAP 2022), Madrid, Spain, March 2022 (**submitted**).

Acknowledgements

Gostaria de agradecer ao Professor Sérgio Matos por me ter incentivado ao longo dos anos a descobrir e explorar cada vez mais esta área. Pela sua disponibilidade, apoio e compreensão. Por ter honrado o seu compromisso e de ter brio em ajudar e ensinar os seus alunos.

Agradecer ao Professor Jorge Costa que sempre se mostrou disponível para fazer os devidos comentários ao trabalho que se veio a desenvolver. Agradecer também pelas suas aulas cativantes de eletromagnetismo e propagação e radiação, e principalmente, o seu entusiasmo.

Agradecer aos restantes intervenientes que durante reuniões ou trocas de e-mail ajudaram a discutir certos assuntos, como é o caso do Professor Carlos Fernandes do Instituto de Telecomunicações e Nelson Fonseca da European Space Agency (ESA).

We would also like to express our gratitude to P. S. Simon, for the sharing of his application for the analysis and synthesis of Rotman Lenses. This has allowed the project to advance in a faster and more efficient way. It was also relevant to have a way of confirming the analytical results with an excellent and well documented application.

Agradecer aos meus pais e avós, pelo apoio imprescindível, tanto financeiro como emocional, e pelos valores que me transmitiram ao longo da minha vida, que fazem parte do que sou hoje. Ao meu irmão que sempre tentei servir de exemplo e ser uma pessoa melhor. À minha namorada pelo apoio e carinho prestado, sempre se mostrando como um pilar para mim ao longo do desenvolvimento desta tese.

Aos meus amigos, tanto dentro e fora da vida académica, cuja experiência tive de confraternizar, de rir, de espairecer e aprender. Agradeço a sua companhia e apoio.

To all of you, my most sincere “Thank you”.

A todos, o meu mais sincero “Obrigado”.

Resumo

Existem vários serviços associados a comunicações satélite e 5G que utilizam as bandas de frequência K e K_a. As redes de formação de feixes são componentes cruciais para alcançar a flexibilidade e agilidade necessárias nestes sistemas. Recorremos à antena clássica de lente de Rotman, como uma solução rentável para ultrapassar as principais limitações de outros tipos de redes formadoras de feixes, nomeadamente largura de banda, complexidade e tamanho.

A principal motivação para esta escolha é a ampla largura de banda, compatível com as bandas de frequência K/K_a de comunicações de satélite, e a utilização de meio de propagação ar/vácuo na secção de guia de onda de placa paralela para evitar perdas dielétricas associadas às implementações de microstrip.

Desenvolvemos uma transição entre um *double ridged waveguide* e um *parallel plate waveguide*, capaz de realizar uma operação de banda ultra larga (16-40 GHz). Após uma avaliação inicial, montámos uma lente de Rotman totalmente operável utilizando uma crista dupla padrão K/K_a (WRD180). O desenho apresentado consiste numa lente de Rotman 13×7, com um alcance de varrimento de $\pm 50^\circ$, operando entre 16 e 40 GHz, validada através de simulações de onda completa.

Apresentamos um desenho capaz de explorar totalmente a largura de banda do guia de onda de crista dupla, com varrimento de feixe largo, superando trabalhos anteriores.

Palavras Chave

5G, Satellite on the move, Beam forming networks, Rotman Lens, Double Ridge Waveguide, K/K_a Band

Abstract

Several services associated with satellite on the move and 5G applications are populating the K and K_a frequency bands. Beam forming networks are crucial components for achieving the necessary beam flexibility and agility of these systems. We resort to the classical antenna Rotman Lens, as a cost-effective solution for overcoming the main limitations of other types of beam forming networks, namely bandwidth, complexity, and size.

The main motivation for this choice is the wide bandwidth, compatible with the K/K_a satcom frequency bands, and the use of air/vacuum propagation medium in the parallel plate waveguide section to avoid dielectric losses associated with microstrip implementations.

We developed a transition between the double ridge waveguide and the parallel plate waveguide, capable of performing a ultrawide band operation (16-40 GHz). After an initial assessment, we assembled a fully operable Rotman Lens antenna using a standard K/K_a double ridge (WRD180). The presented design consists of a 13×7 Rotman Lens, with a scanning range of $\pm 50^\circ$, operating between 16 and 40 GHz, validated through full-wave simulations.

We present a design capable of fully exploiting the ridge waveguide bandwidth with wide beam scanning, outperforming previous works.

Keywords

5G, Satellite on the move, Beam forming networks, Rotman Lens, Double Ridge Waveguide, K/K_a Band

Index

List of Figures	I
List of Tables	III
List of Acronyms	V
Introduction	1
1.1. Motivation	1
1.2. State of the art.....	2
1.2.1. Design of the Rotman Lens	3
1.2.2. Feeding Network	4
1.2.3. Feeding Rotman Lens with Power divider	7
1.2.4. Continuous Parallel plate waveguide delay lens	7
1.2.5. Circularly Polarized Rotman Lens	8
1.3. Objective.....	9
1.4. Work highlights	9
Physical principles and Synthesis	11
2.1. Introduction	11
2.2. Rotman Lens concepts and formulas.....	12
2.2.1. Beam Ports	13
2.2.2. Array Ports	14
2.2.3. Transmission Lines	15
2.3. Synthesis and analysis (MATLAB Application).....	16
2.4. Model Assemble	19
2.4.1. CST – Microwave Studio macro	19
2.4.2. Full model assembly.....	20
Initial Assessment	21
3.1. Introduction	21

3.2.	Rotman Lens Design	21
3.3.	Feeding Network	22
3.4.	Rotman Lens Full-Wave Simulation	26
3.5.	Conclusions	27
Rotman Lens Operating in the Full K/K_a Band		29
4.1.	Introduction	29
4.2.	RL Design.....	29
4.2.1.	Geometry	29
4.2.2.	Double Ridge Waveguide to PPW Transition.....	30
4.2.3.	Considerations and optimizations	31
4.3.	Assembling of the Rotman Lens	33
4.4.	Numerical results and discussion	34
Conclusions		39
5.1.	Main achievements	39
5.2.	Future work.....	40
References		41
Attachments		45
A.	Manual MATLAB Application	45
B.	Macro CST	49
C.	Submitted Article for EuCAP 2022	56

List of Figures

Figure 1: Geometry and design parameters of the Rotman Lens [3].	3
Figure 2: Straight flares, feed design from [9].	6
Figure 3: Curved flares, feed design from [8]. Top View (a) and Cross Section (b) of the Lens Feed Network.	6
Figure 4: Mixed flares, feed design from [4], [10].	6
Figure 5: Cross Section of a waveguide Rotman lens geometry [30].	7
Figure 6: Design of a continuous parallel plate waveguide lens-like beamformer at K _a -band. (a) 3D PPW beamformer design and (b) PPW lens close-up view [35].	8
Figure 7: Side view of the QOBF connected to the septum array [36].	8
Figure 8: Ray Geometry of the Rotman Lens.	12
Figure 9: Geometry for determining the BPs coordinates.	13
Figure 10: MATLAB Application – Rotman Lens.	16
Figure 11: (a) Component Position Preview; (b) Exporting port position; (c) Normalized Array Factor; (d) Phase Error Preview.	17
Figure 12: Transmission line data.	18
Figure 13: Transmission Lines	18
Figure 14: Feed Model.	19
Figure 15: Macro (Imports) CST – Microwave Studio.	19
Figure 16: Flowchart of the automated system developed.	20
Figure 17: Beam and array contour phase centres [MATLAB], adapted from Simon, P.S. [26]	22
Figure 18: Single Feeding Port (adapted from [4])	23
Figure 19: Simulated E-Fields of a single feed at 24.15 GHz.	23
Figure 20: Simulated S ₁₁ for a single feed port.	24
Figure 21: Simulated E-Fields of a single feed with extended side walls at 24.15 GHz	24
Figure 22: Simulated S ₁₁ for a single feed port with extended side walls at 24.15 GHz.	24
Figure 23: Model to evaluate mutual coupling between adjacent ports. Beam port 1 (left), beam port 2 (middle), and port 3 (right).	25
Figure 24: Simulated S parameters of the 3 adjacent feeds	25
Figure 25: Simulated E-Fields at 17.3 GHz for beam port 1 (left), beam port 2 (middle), and port 3 (right)	26

Figure 26: Simulated E-Fields at 24.15 GHz for beam port 1 (left), beam port 2 (middle), and port 3 (right)	26
Figure 27: Simulated E-Fields at 31 GHz for beam port 1 (left), beam port 2 (middle), and port 3 (right)	26
Figure 28: S-parameters from 17.3 to 31 GHz, for Beam Port 1	27
Figure 29: S-parameters from 17.3 to 31 GHz, for Beam Port 2	27
Figure 30: S-parameters from 17.3 to 31 GHz, for Beam Port 3	27
Figure 31: Profile of the designed Rotman Lens.....	30
Figure 32: (a) Geometry of the design Ridge to PPW transitions with $a = 7 \text{ mm}$, $b = 6.8 \text{ mm}$, $c = 3.4 \text{ mm}$, $d = 14.9 \text{ mm}$. (b) Transitions in the Rotman lens.....	31
Figure 33: RL with absorbent filled, in between each port.	32
Figure 34: S-Parameters of the APs with $\beta = 1$	32
Figure 35: S-Parameters of the APs with $\beta = 0.97$	33
Figure 36: 3D Model representation [CST]: (a) side view; (b) top view	33
Figure 37: Amplitude (a) and phase (b) field distribution inside RL for 30 GHz for three different beam port excitations.....	34
Figure 38: Field magnitude distribution. Top row represents BP1 and lower row BP7 (Centre)	35
Figure 39: S-parameters between all beam ports 16 to 40 GHz.....	35
Figure 40: S-parameters between all array ports 16 to 40 GHz.	35
Figure 41: Phase at the output ports of the TLs (each dot corresponds to a different TL) considering multiple frequencies for the central port (a) and most scanned one (b).	37
Figure 42: Array factors for ports 1,3 and 7 at 18 GHz and 30 GHz. Comparison of the full-wave simulations (solid lines) with the case of ideal linear phase variations and constant amplitude (dashed lines).....	37
Figure 43: Antenna power efficiency. Green line represents Beam Port 1(Extremity), and the red line represents Beam Port 7 (Centre)	38

List of Tables

Table 1. Design parameters for the Rotman Lens	22
Table 2. Feed design values	23
Table 3 – Design parameter of the Rotman Lens	30
Table 4 - Beam direction and average phase error for sequential beam port excitation (see Figure 32 (b)), at 18 GHz, 30 GHz, 40 GHz.	36
Table 5 - Comparing different broadband Rotman lens designs.....	40

List of Acronyms

AP	Array Port
BFN	Beam forming Network
BP	Beam Port
CP	Circular Polarization
FDTD	Finite Difference Time Domain
GO	Geometrical optics
GUI	Graphical User Interface
LEO/MEO	Low/Medium Earth orbit
PMU	Phase Management Unit
PPW	Parallel plate waveguide
QOBF	Quasi-optical beamformer
RE	Radiating Element
RL	Rotman Lens
TEM	Transversal Electromagnetic Mode
TL	Transmission Line
TTD	True Time Delay
WRD	Waveguide, Rectangular Double ridged

CHAPTER ONE

Introduction

1.1. Motivation

With the advent of a new generation of mobile communications, 5G, a new interoperability between different technologies and networks arises. In particular, satellite communications, traditionally thought as a standalone system, become part of this global network. The goal of this endeavour is to provide a seamless wireless experience across the entire globe, connecting everyone, everything and everywhere [1]. 5G will need uninterrupted coverage that terrestrial networks on its own cannot guarantee. Satellite systems bring solutions that enhance 5G communications, ending low coverage areas and signal blocking by buildings or terrain. Satellite missions are increasingly being carried out as they become more cost-effective. In fact, a new space race is taking place among tech companies, that started deploying Low/Medium Earth orbit (LEO/MEO) satellite constellations to deliver high-speed data rates services. It is expected, in the next few years, for thousands of satellites to be further launched, forming mega-constellations. This high demand requires new low-cost broadband antenna solutions that can foment the massification of this technology.

In the past few years, there has been several developments on array antennas for small-space platforms targeting LEO/MEO communication satellite constellations. The trend is for the increase of the operation frequency for achieving the necessary capacity, however, this impacts the antenna complexity and cost [2]. The challenge is to find cost-effective solutions for broadband antennas capable of performing multibeam and/or wide beam scanning.

This study intends to contribute to this development by optimizing and improving existing promising technologies. More specifically, this work revisits the design of Rotman Lens (RL) antennas for the new generation of satellite communications at K/K_a band using double ridge waveguide (WRD) technology. The general idea is to benefit from the wide bandwidth of ridge waveguides and aim for an all-metal design, suitable to survive the harsh environment of space. The Rotman Lens antenna is one of the most popular types of constrained lens. It offers a combination of broadband operation, compactness and wide-angle beam steering, as a solution for a wide range of applications related with 5G and satellite communications [3]. In fact, the Rotman Lens design is currently being investigated as viable solution for the emergent mega-constellations in low and medium Earth orbit (LEO/MEO) [4].

1.2. State of the art

Rotman Lens is a classical constrained lens [5]–[7], that is still being widely researched for continuous improvements and adaptations to current technological developments [4], [8]–[10]. Constrained lenses are a special group of multibeam antenna arrays or beamforming networks. The name constrained comes from the fact that a wave incident on one face of the array does not necessarily obey Snell's law when passing through the lens, although Snell's law can be applied to optimize the lens performance [11]. This antenna uses free-space wavelength signal injected into a geometrically configured system. As a beam forming network (BFN), the radiation of each antenna input port is channelled to multiple output beam ports that collectively form the beam. The direction of the beam shifts as different input ports are used. There exist multiple simultaneous beams when an array of N elements is connected to a beamformer with M beam ports, where N and M may be different. In general, with a lens BFN, since geometric optics is applied, the ray paths have the same lengths. This means, in theory, that the angles of each beam tilt remain the same, independent of frequency. Although the angles are fixed, the beamwidths, and consequently the crossover levels, change with frequency [12].

For the input ports we call them beam ports (BPs), for the output ports we call them array ports (APs). The connection between the input and output ports is done through a parallel plate waveguide (PPW) in the TEM regime, which explains the intrinsic broadband behaviour of the lens. The positions of the input and output ports are obtained from Geometric Optics (GO) analysis. This lens can be designed with up to four degrees of freedom [13]. In this work, the common three degrees are chosen [7].

Some main advantages of using the Rotman Lens design are [3]:

- The direction of the antenna's beam can be adjusted easily to the desired angle just by switching the input port. It distinguishes itself from continuous beam-steering techniques using components such as thermal phase shifters, which are slow and highly sensitive to environment temperature.
- They produce multiple beams, which can be steered without changing the orientation of the antenna.
- Microwave lenses are the ones who support low-phase error, wideband, and wide-angle-scanning.
- They are a true time delay (TTD) device producing frequency independent beam steering.

The main drawbacks of this antenna is that the size of the beamformer is linked to the size of the array aperture [10].

1.2.1. Design of the Rotman Lens

The development of the Rotman Lens was pushed forward with the work presented by W. Rotman and Turner, in the 1960s [7]. The lens achieved a two-dimensional scanning and TTD architecture by using a parallel plate transmission with cavities fed by rectangular waveguides. It was designed with three focal points and enhanced previous designs, such as Ruze Lens. Rotman and Turner's work also improved coma aberrations and off-axis phase distortions, by the use of general lens design principles developed by Gent [7].

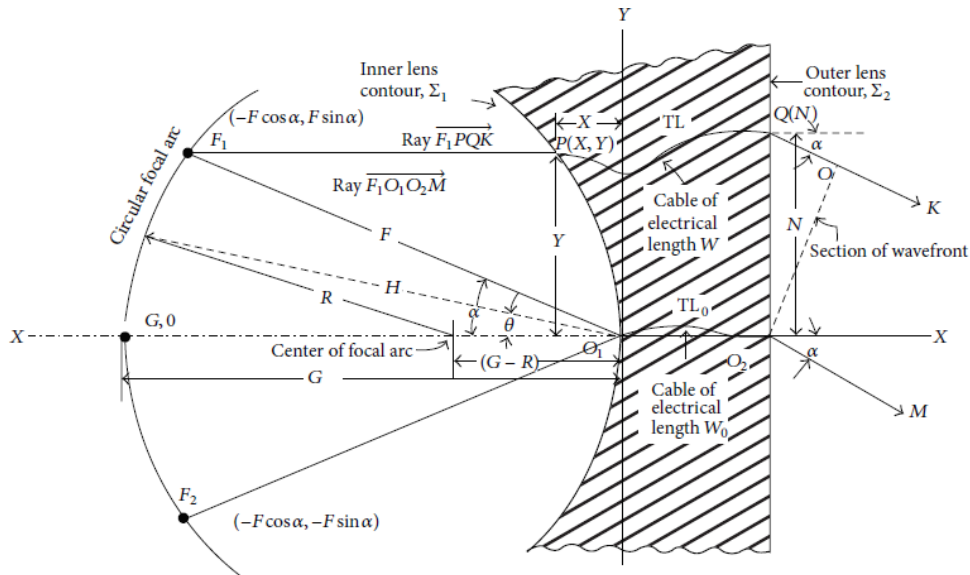


Figure 1: Geometry and design parameters of the Rotman Lens [3].

Figure 1 depicts the geometry and design of a Rotman Lens. As W. Rotman explained, the contour Σ_1 is defined by two coordinates (X, Y) that are specified relative to a point O_1 on the central axis of the lens. Elements on the straight contour Σ_2 are similarly determined by the single coordinate N , measured relative to the point O_2 . O_1 and O_2 lie on the contours Σ_1 and Σ_2 , respectively, and are connected by a transmission line (TL) [7]. Finally, the BPs are placed along the focal arc represented above. The result of this procedure is a lens with three perfect focal points, corresponding to angles of $\pm\alpha$ and 0° . This design was simple and effective in comparison with more complicated designs that tried to reproduce a symmetrical lens, with respect to the beam and inner lens contours [14].

Other major optimizations were made by different authors, in the 1980s. It was shown that the lens port width could impact the reflection coefficient of the port. This results in degradation of the lens amplitude and phase distributions [15]. One solution, at the time, was the application of an isolated power combiner at the lens port [3]. Based on the concept of RL design, an author named Katagi proposed an improved design in 1983. This innovative design helped reducing the size on the lens, by applying a refocus method that also lowered the phase errors of the original design [16]. Another important group of authors named, Musa and Smith, in the 80s, worked together to design solutions for the side wall reflections, by introducing side wall absorption methods [17]. They also developed a theoretical model to predict the primary amplitude distribution across the APs of the lens [18].

The design was further explored by Hansen, in the 90s, who did a major breakthrough in his work presented as *Design Trades* [19]. Some of his other projects were also important, defining the Rules of Thumb for the RL design and bringing this antenna to the mm-wavelengths [20]. Hansen defined six basic parameters to design the lens and explained the effect of each parameter in detail, plus another one that was derived from two basic parameters. His design, like ours, assumed to be air filled and the beams were scanned into free space.

In the early XXI century, there is still a lot that can be optimized, not only the beam ports and array ports, but also the side walls [21]. Several studies were made in this time period that tried to optimize the design, from modifying the lens contour to a more elliptical shape [16] to beam pointing techniques [22]. There are still recent studies that enhance the lens performance, mostly applied to the GO analysis [23], [24], [25]. In 2004, the first reported GUI specially designed for the Rotman Lens antenna was developed, by Peter Simon [26].

Although there is more literature about optimization along the history of the model, it was only chosen literature suitable to be applied in a full all-metal approach.

The next subsections will demonstrate the innovative designs developed in the scope of this thesis.

1.2.2. Feeding Network

The design of the waveguides is just as important as the lens design. They bring energy to our system and they should be meticulously designed in order to bring the lowest losses possible, and spill over. They should have a good matching when embedded in our system. Another aspect to be taken into consideration is the fact that there are several ports next to each other, therefore the relationship between them must be studied. Our approach will be more inclined to ridged gap waveguides. This choice was made because high order waveguides, e.g. single

[27] or double ridged waveguides [8], [9], allow for the propagation of TEM waves and thus incorporate a larger bandwidth. Nevertheless, the symmetric nature of the TEM and the presence of ridge complicate the integration in the lens [8].

A ridged waveguide is a simple rectangular or circular waveguide with a ridged protruding into the centre of the waveguide from the top wall or bottom wall, or even both walls like our design. The ridges are parallel to the wall of the waveguide. They can offer a set of interesting characteristics with advantages and disadvantages [28].

Advantages:

- Impedance Matching: The ridges decrease the waveguide characteristic impedance, which can be useful for impedance matching.
- Lower cut-off frequency: The right implementation of ridges to a simple waveguide will result in a low cut-off frequency of its fundamental mode. This will result in having a small cross section of the ridge waveguide, which presents an opportunity for compact designs.
- Compactness: In the context of Rotman Lenses, where microstrip lines are more commonly used, ridged waveguides can offer a compact solution where planar transmission lines are not able to handle some power levels. Although power handling of ridged waveguides is not as good as of rectangular waveguides, it is better than microstrip lines.
- Bandwidth: Ridged waveguides also offer higher bandwidth in comparison to the conventional waveguides.

Disadvantages:

- Ohmic Loss: The ohmic losses are greater in ridged waveguides than rectangular waveguides, although they can be optimized.
- Power Handling: Because of the ridges, the power handling is lower than of the rectangular waveguide. Although some trade-offs can be made, we will focus more on the insertion design of the feed in the parallel plate waveguide, and we aim to use a commercialized version of a ridged waveguide.

According to P. Knott *et. al* [8], the bandwidth of rectangular waveguides can be limited to approximately one octave due to the propagation of higher order modes at higher frequencies. To increase the frequency range, a ridged design allows the propagation of a quasi-TEM mode and may be used for feeding a lens over a large frequency range.

In addition, an important note from K. V. Hoel *et. al* [9], says that the PPW should have a spacing of less than half of the guided wavelength in order to stimulate only a TEM propagation mode within the cavity.

To clarify, other adaptations can be made in order to improve the response of the feeds, like adding a back-cavity and rounding the end of the ridges or even increasing the diameter of the inner conductor of the coax [29]. However, this is not the focus of this work.

In this section, we present three cases of WRD feeds, some already implemented in a RL. The main difference between them is how the flares are designed, one has straight flares (Figure 2), another curved flares (Figure 3) and the last one has mixed flares (Figure 4).

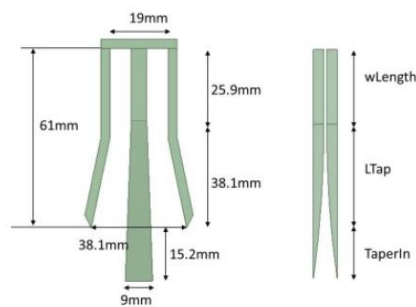


Figure 2: Straight flares, feed design from [9].

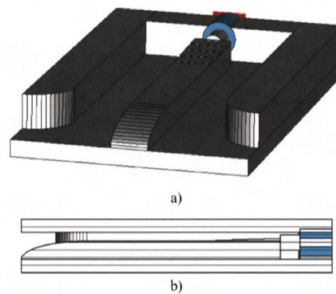


Figure 3: Curved flares, feed design from [8]. Top View (a) and Cross Section (b) of the Lens Feed Network.

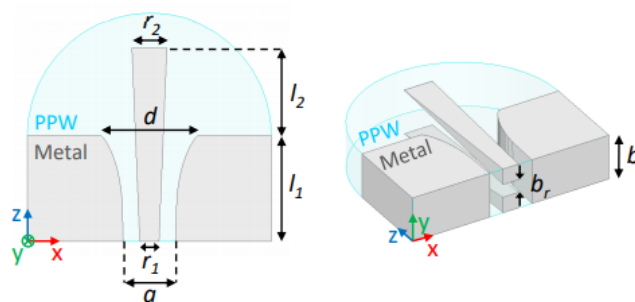


Figure 4: Mixed flares, feed design from [4], [10].

1.2.3. Feeding Rotman Lens with Power divider

This model incorporates a non-TEM parallel-plate mode of propagation, which limits the bandwidth. It incorporates rectangular waveguide feeds around the lens periphery, as well as power dividers [30], as shown in Figure 5.

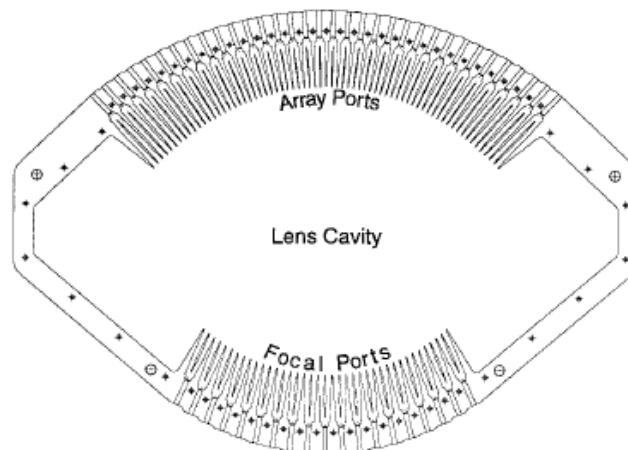


Figure 5: Cross Section of a waveguide Rotman lens geometry [30].

The design uses a folded “magic tee” incorporated in each feed line to provide a 3dB power divider, which splits the feeds into two smaller in-phase apertures. This design was later implemented to support a Rotman Lens antenna array operating at 94 GHz [31], and another antenna that operates at frequencies between 33GHz and 37GHz [32].

1.2.4. Continuous Parallel plate waveguide delay lens

This next model is based on GO and analyses a continuous PPW [33]–[35]. This beamformer transforms the cylindrical wave launched by one of the primary feeds, propagating inside the PPW section, into a nearly plane wave radiated in free space by the radiating horn, and vice versa (Figure 6). These lenses use a polynomial shaped delay to demonstrate low phase aberrations and performance.

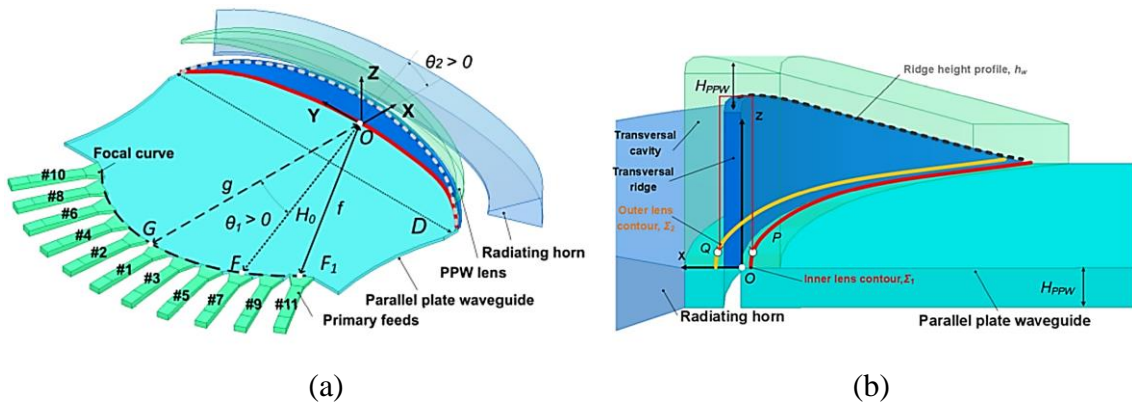


Figure 6: Design of a continuous parallel plate waveguide lens-like beamformer at K_a -band. (a) 3D PPW beamformer design and (b) PPW lens close-up view [35].

This antenna reduces the size of a common Rotman Lens by, instead of having array ports and transmission lines, it has a delay lens at the end.

1.2.5. Circularly Polarized Rotman Lens

This work describes a way to induce a circular polarization in a PPW. It uses a septum polarizer based on a stepped profile. It was also designed to operate at K_a -Band (27.5 – 30.0 GHz), making it an appealing approach for future work to be based on. Generally, circular polarization (CP) is required for SatCom applications in K_a -Band [36]. As depicted in Figure 7, the paper presents a continuous PPW quasi-optical beamformer (QOBF) with an array of septum polarizers to generate circular polarization.

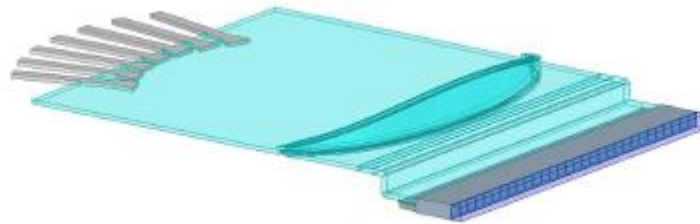


Figure 7: Side view of the QOBF connected to the septum array [36].

1.3. Objective

This work intends to explore the main advantages of the Rotman Lens for developing a compact, low cost, wide beam scanning antenna solution for new generation of satellite systems capable of operating in the entire K/K_a band (16-40 GHz). A fundamental part of this design is the transition between the input and output ports of the antenna and the parallel plate waveguide (PPW) that compose the body of the lens, which should be capable of operating in the intended bandwidth. We already found in the literature some examples that achieve good results in close bands, like K_u, Q, V and W found in [4], [9], [10] and [31]. However, larger bandwidth, wider scanning angles and higher number of input and output ports will be considered in this work, further exploring the potential of ridge waveguide based Rotman lenses. One should stress that there are few studies considering ridged waveguides for the implementation of the Rotman lens concept [8], [9].

The general objective of this work is supported by specific goals that will guide the layout of this document, namely:

- Create a systematic tool for generating and analysing a complete Rotman Lens. This framework is fundamental for allowing an iterative optimization process using geometric optics and full-wave results.
- Design of a transition between PPW and WRD capable of operating in the entire K/K_a satellite band (17.3 GHz-31GHz) [37].
- Prove the viability of the designed transition for an initial Rotman lens configuration with a low number of input and output ports.
- Optimize a RL design for reducing reflections and phase errors considering wide beam scanning and extending the operation frequency to the entire K/K_a bands (16-40 GHz).

1.4. Work highlights

Our methodology starts by selecting the papers from the current state of the art that suits our application, full metallic solution with wide bandwidth. It is important to note that this type of antenna is commonly used in a microstrip setup. Most of those setups were discarded unless they had something adaptable to our antenna. The second step was the design of an automatic process of designing Rotman lens from basic principles (GO analysis) until a complete full-wave model of the lens, that includes the transmission lines (which is usually omitted in available studies on the literature).

There are several GO analyses studies around the Rotman Lens. Therefore, we had to choose the theory that best suits this work, having chosen Hansen's work as a starting point [19].

To assess the viability of our work, we confirmed our calculations with the tool given to us by Peter Simon [26], his own simulation tool designed in MATLAB. His application is one of the first reported GUI specially designed for Rotman Lens antennas. His lens design software is verified by comparing its results with numerical analysis of Rotman Lens.

Afterwards, we replicated a model from a study that is close to the approach we were going to take [9]. Being familiar with the construction of a RL antenna, we shifted our attention to make it work on the desired K/K_a Band. Most of the effort has been put into building our solution and optimizing it. We evaluated our solution by doing a full wave analysis, resorting to the software CST – Microwave Studio.

This work started with the revision of the literature related with Rotman Lens, which was used to establish an initial design to work on [38]. This design was thus improved to match our operating bandwidth. There are some potential topics of research when working with this antenna:

- Lens Design – Geometrical Optics (GO) Analysis;
- Feeding Network Design;
- Sidewalls Design;
- Radiating elements.

This thesis is organized as follows. In Chapter One, an introduction to the thesis is given and the state of the art is presented, as well as our objectives for this work. In Chapter Two, the basic concepts and physical principles of the lens are explained, as well as how the antenna is synthesized. In Chapter Three, an initial assessment is made in order to develop a transition from the WRD to the PPW that can work on the desired K/K_a Band. In Chapter Four, we present our complete design of the RL, capable of operating in the entire K/K_a Band (16-40 GHz). Finally, in Chapter Five, the conclusions are drawn, and future work is summarized.

CHAPTER TWO

Physical principles and Synthesis

2.1. Introduction

In this chapter, the basics of this work are described from the theoretical formulation to the synthesis of the antenna. The Rotman Lens antenna is one of the most popular types of constrained lens. The combination of the broadband operation, compactness and wide-angle beam steering makes this type of antenna an appealing solution for a wide range of applications related with 5G and satellite communications. This classical antenna [7] is still being widely researched for continuous improvements and adaptations to current technological developments [4], [8], [9].

As a BFN, the radiation of each antenna input port is channelled to multiple output beam ports that collectively form the collimated beam. The direction of the beam shifts, as different input ports are used. The connection between the input and output ports is done through a PPW in the TEM regime, which explains the intrinsic broadband behaviour of the lens. Moreover, the radiating elements of the antenna are connected to the array ports by TL with specific lengths (as depicted in Figure 8). The positions of the input and output ports are readily obtained from GO analysis. However, a careful design is required for the feeding network, which will limit the lens performance.

The first design aspect is related with the number of input and output ports of the lens, which depends on the intended application. There is a trade-off between the feed spacing and port isolation. On the one hand, closer feeding ports correspond to a higher beam density. On the other hand, closer feeding ports will increase the coupling between adjacent ports. Moreover, the physical aperture of the feeding elements will further constrain the array spacing.

Another crucial step for this design is the bandwidth of the TLs and the transition to the PPW. In the context of satellite communications, RL are particularly appealing for the space segments, being currently investigated as a viable solution for the emergent mega-constellations in LEO/MEO [4]. In this case, an all-metal design is best suitable to survive the harsh environment of space. In this chapter, we will focus on the design of this type of antenna, aiming for a broadband behavior starting in the satellite Rx K band (min. 17.3 GHz) until the Tx K_a band (max. 31 GHz) [37]. Ridge wave technology emerges as a natural option for achieving such a wideband using only metal. In fact, several recent works have explored this configuration [4], [9], however, not in this bandwidth.

The synthesis of the Rotman Lens is divided into several parts, as told in the research methodology. To explain the synthesis of this antenna, the several parts are split one by one, to clarify which points have to be considered, their problems and how those were solved.

2.2. Rotman Lens concepts and formulas

As already mentioned throughout the thesis, the Rotman Lens is a constrained lens, based on GO. In this section we will talk about how it is elaborated in a more mathematical way. In the figure below (Figure 8) it is presented a simplified schematic of this lens. One can also further interpret Figure 1 to follow the analysis, being this the initial schematic for W. Rotman's design.

This constrained lens has its paths' lengths and elements' positions previously calculated from the Beam Ports (BPs), through the Array Ports (APs) and Transmission Lines (TLs), ending at the Radiation Elements (REs). The character w represents the length of the TLs. The lens is composed of two “arcs”, on the left arc the BPs are placed side by side, as well as for the APs on the right arc that is called the “Inner Lens Contour”. The REs are placed along the Array Axis (linear plane $x = f_1$). Since this was the first time we worked with this type of antenna design, we decided to choose a linear plane to position the REs, as it simplifies the design and assembly. Other setups will be explored in the future.

Δd represents the distance between each RE. It is represented in W. Rotman's work as N [7], as explained in section 1.2.1. and observed in Figure 1. In Hansen's studies, it is represented as y_3 [19]. In our work, we used Δd for the analysis to be more intuitive for the reader.

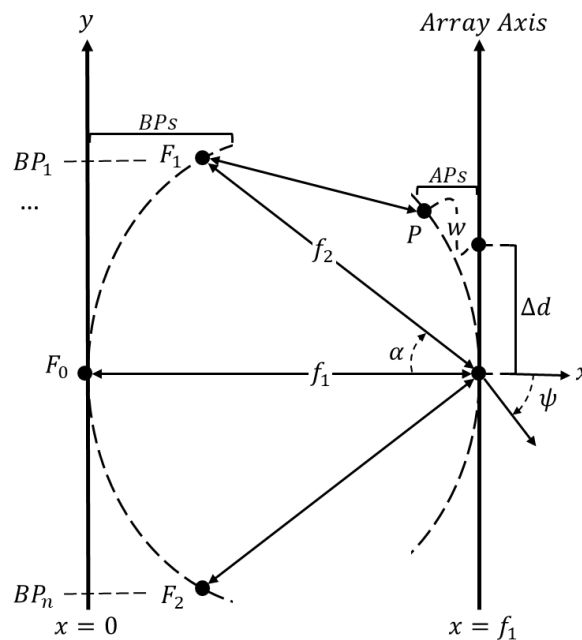


Figure 8: Ray Geometry of the Rotman Lens.

Expanding the square and normalizing the expression with f_1 as we do in most of our work, whereby $\rho = R_{BPS}/f_1$, we get:

$$\rho = 1 - \frac{1-\beta^2}{2(1-\beta C)} \quad (2.2)$$

Applying the Law of Sines to determine ϕ , we have:

$$\phi = \sin^{-1} \left(\frac{1-\rho}{\rho} \sin \alpha \right) \quad (2.3)$$

The angles can be manipulated to get δ :

$$\delta = \pi - \eta = \pi - [\pi - (\alpha + \phi)] = \alpha + \phi \quad (2.4)$$

Finally, we obtain the points:

$$X_b = \frac{x_b}{f_1} = \frac{R_b - R_b \cos \delta}{f_1} = \rho(1 - \cos \delta) = \rho[1 - \cos(\alpha + \phi)] \quad (2.5a)$$

$$Y_b = \frac{y_b}{f_1} = \frac{R_b \sin(\delta)}{f_1} = \rho \sin(\delta) = \rho \sin(\alpha + \phi) \quad (2.5b)$$

2.2.2. Array Ports

In this section we calculate the position of each AP. The following explanation can be followed visualizing Figure 8. The APs are the ports that receive the energy from the BPs to subsequently be emitted by the REs. For ease of understanding, we will call the focal point where the APs are positioned $P(x_a, y_a)$. The calculation for the position of the APs requires a more laborious and extensive work. We follow the traditional design rules starting with three focal points. Two of them are symmetric, F_1 and F_2 , with the respective coordinates of $(f_1 - f_2 C, f_2 S)$ and $(f_1 - f_2 C, -f_2 S)$, where S and C are simplifications presented in equation 2.7.

Now, we can apply geometric optics to generate the equations that correspond to the optical path-length equality between a general ray and the ray through the origin:

$$\|\overline{F_1 P}\| + w + \Delta d \sin \psi = f_2 \quad (2.6a)$$

$$\|\overline{F_2 P}\| + w - \Delta d \sin \psi = f_2 \quad (2.6b)$$

$$\|\overline{F_0 P}\| + w = f_1 \quad (2.6c)$$

Now that we have the ray paths defined, we can define the path lengths of each focal point to point P . For a simplified presentation, let us assume that:

$$C = \cos(\alpha); S = \sin(\alpha) \quad (2.7)$$

The length of the ray paths is expressed in terms of coordinates of points, obtaining:

$$\|\overline{F_1P}\|^2 = (f_1 - f_2C - x_a)^2 + (f_2S - y_a)^2 \quad (2.8a)$$

$$\|\overline{F_2P}\|^2 = (f_1 - f_2C - x_a)^2 + (f_2S + y_a)^2 \quad (2.8b)$$

$$\|\overline{F_0P}\|^2 = x_a^2 + y_a^2 \quad (2.8c)$$

Equalizing the equations and substituting $\sin \psi = \gamma \sin \alpha = \gamma S$, just as Hansen defined these parameters [19], we get:

$$(f_1 - f_2C - x_2)^2 + (f_2S - y_2)^2 = (f_2 - w - \Delta d \gamma S)^2 \quad (2.9a)$$

$$(f_1 - f_2C - x_2)^2 + (f_2S - y_2)^2 = (f_2 - w + \Delta d \gamma S)^2 \quad (2.9b)$$

$$x_a^2 + y_a^2 = (f_1 - w)^2 \quad (2.9c)$$

Finally, we normalize all the parameters to f_1 , as we do in all this thesis:

$$\beta = \frac{f_2}{f_1}; \quad \zeta = \frac{\Delta d \gamma}{f_1}; \quad W = \frac{w}{f_1}; \quad X_a = \frac{x_a}{f_1}; \quad Y_a = \frac{y_a}{f_1} \quad (2.10)$$

We are left with the final point position of:

$$X_a = \frac{(\beta-1)W - \frac{1}{2}\zeta^2 S^2 + (1-\beta)C}{1-\beta C} = 1 - \frac{\frac{1}{2}\zeta^2 S^2 + (1-\beta)W}{1-\beta C} \quad (2.11a)$$

$$Y_a = \frac{-\zeta SW - \beta \zeta S}{\beta S} = \zeta \left(1 - \frac{W}{\beta}\right) \quad (2.11b)$$

2.2.3. Transmission Lines

The TLs are a vital part of this antenna, their lengths are calculated in a way where the optical path-length equality, demonstrated in the set of equations 2.6 (a-c), is assured. This equality is what makes the antenna frequency independent. If an extra length is added to one of the TLs, it has to be added to all of the TLs so the equality preserved. The path length of each TL, represented as w , can be given by a quadratic equation, which can be solved by exploring equation 2.9c. Expanding the square of equation 2.9c and normalizing it for f_1 we have:

$$X_a^2 + Y_a^2 = 1 - 2W + W^2 \quad (2.12)$$

The quadratic expression can be solved with the resort of the expressions achieved in 2.11(a-b). The results are:

$$aW^2 + bW + c = 0 \quad (2.13)$$

$$a = 1 - \frac{(1-\beta)^2}{(1-\beta C)^2} - \frac{\zeta^2}{\beta} \quad (2.13a)$$

$$b = -2 - \frac{2\zeta^2}{\beta} + \frac{2(1-\beta)}{1-\beta C} - \frac{\zeta^2 S^2 (1-\beta)}{(1-\beta C)^2} \quad (2.13b)$$

$$c = -\zeta^2 - \frac{\zeta^2 S^2}{(1-\beta C)} - \frac{\zeta^4 S^4}{4(1-\beta C)^2} \quad (2.13c)$$

These equations total seven parameters, which their effects are explained in a series of charts in [19].

2.3. Synthesis and analysis (MATLAB Application)

Assembling the lens can be quite laborious. There are several components with specific positions, so there are several calculations to be done to reach our final goal, which is to build the lens. To simplify this process, a tool was developed that allows to make the calculations and show a preview of the lens performance and structure. This application was developed during this project and is illustrated in Figure 10. Part of this application was inspired by the application made by Peter Simon, who shared his published work [26].

The manual for this application is found in the Attachments section at the end of this thesis.

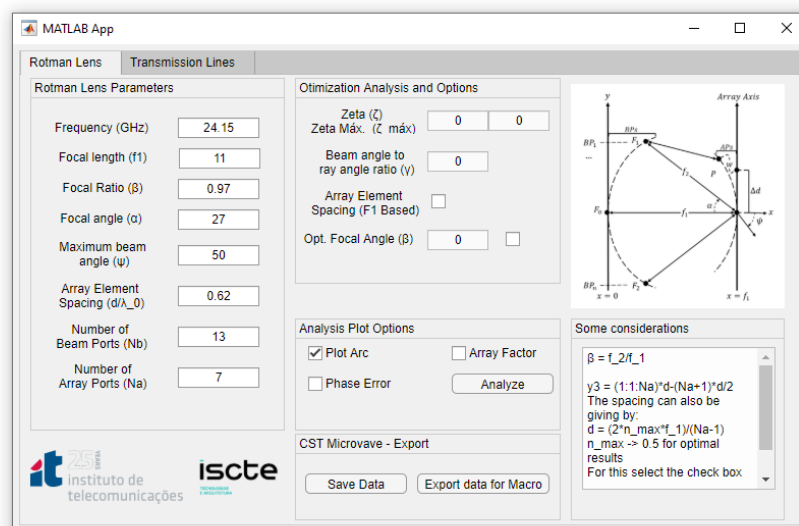


Figure 10: MATLAB Application – Rotman Lens.

The application is divided into two tabs. The first is concerning the GO of the lens. The second tab is relative to the construction of the TLs, although not being fully integrated into the application.

The first tab allows a preview of the overall system from all the ports to the REs, as shown in Figure 11 (a). Additionally, it can export all these values into a *.txt* file (Figure 11 (b)) so that they can be processed in a macro in CST - Microwave Studio, which will be explained in this subsection. Other applications that are included are the calculation of the Phase Error, according to GO, and the Array Factor, as illustrated in Figure 11 (c) and Figure 11 (d). Nevertheless, these two are not yet fully optimized and integrated. It is hoped to further integrate and prepare these tools for as many scenarios as possible.

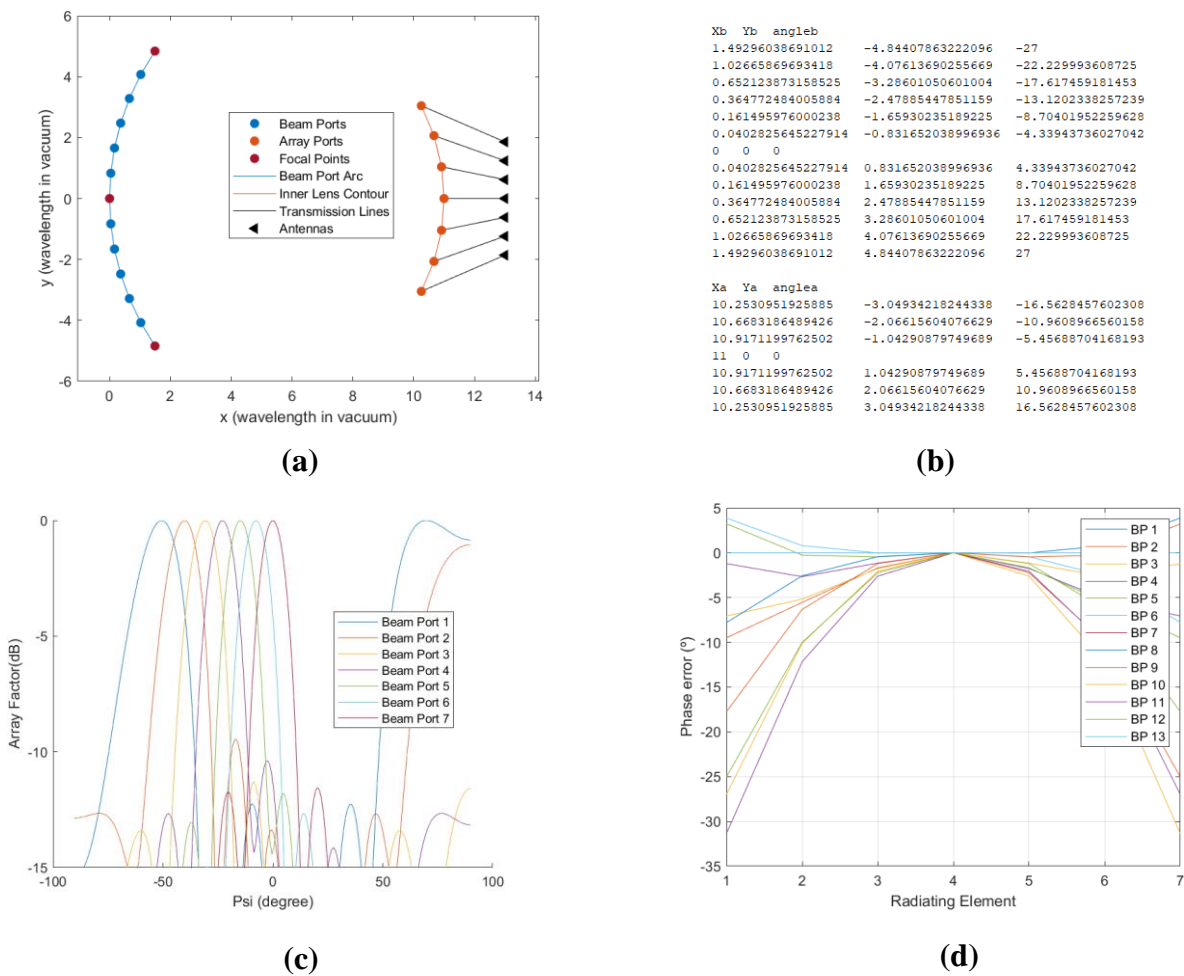


Figure 11: (a) Component Position Preview; (b) Exporting port position; (c) Normalized Array Factor; (d) Phase Error Preview.

The second tab is exclusive for the construction of the TLs. Although it is not fully integrated in the application, it was elaborated separately to obtain better optimization. This function is based on Bézier curves, which allows us to have greater control over the curves. These curves work by having several control points and it is based on these points that these curves are formed. It is possible to calculate the size of these curves by applying an integral to the Bézier functions, which becomes quite important when constructing the TLs for the RLs. We can also have a dynamic point (D_n), that is, a point whose value is a variable where we let MATLAB's solver find the value, so that we get the desired line length, as illustrated in Figure 12.

TL - 1		TL - 2		TL - 3		TL - 4		TL - 5		TL - 6		TL - 7		TL - 8	
X1	Y1	X2	Y2	X3	Y3	X4	Y4	X5	Y5	X6	Y6	X7	Y7	X8	Y8
0.0	5.9	0.0	5.2	0.0	4.4	0.0	3.5	0.0	2.5	0.0	1.7	0.0	0.8	0.0	0.0
2.0	5.9	2.5	5.2	2.5	4.4	2.5	3.5	2.5	2.5	2.5	1.7	2.5	0.8	2.5	0.0
2.3	D_1	3.5	D_2	3.0	D_3	3.4	D_4	3.5	D_5	3.5	D_6	3.2	D_7	4.0	D_8
5.0	7.7	5.0	6.0	4.5	5.5	5.0	4.4	5.0	3.3	5.0	2.2	5.0	1.1	5.0	0.0
5.5	7.7	5.5	6.6	5.5	5.5	5.5	4.4	5.5	3.3	5.5	2.2	5.5	1.1	5.5	0.0
6.0	7.7	6.0	6.6	6.0	5.5	6.0	4.4	6.0	3.3	6.0	2.2	6.0	1.1	6.0	0.0



$$\left\{ \int_c f(x,y) ds = \text{line length} \right\} \text{Solve for } D_n \text{ (MATLAB)}$$

Figure 12: Transmission line data.

Another important point is the fact that we can visualize how these TLs will look, so that they do not get on top of each other. Therefore, to predict these cases a plot of the lines side by side is made, as shown in Figure 13. The Lower/Upper Bounds represent the feed's width. The curves represent each individual TL with a different colour associated. Each TL has circles associated to them, which represent the control points for each TL.

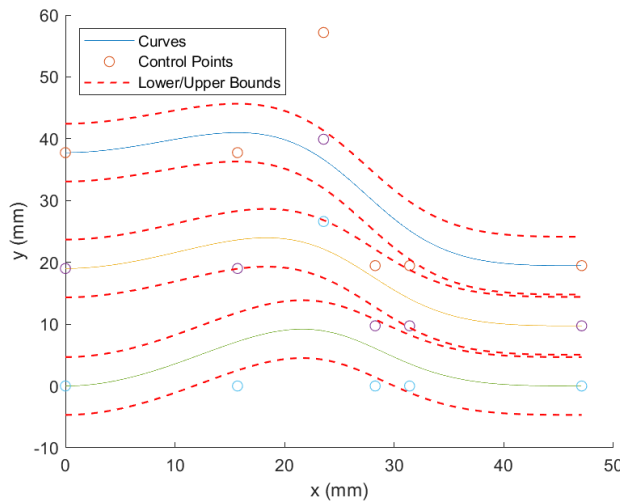


Figure 13: Transmission Lines

2.4. Model Assemble

2.4.1. CST – Microwave Studio macro

The constant modelling of these systems becomes a very time-consuming process, so we resort to the CST – Microwave Studio macro system to automate this whole process. For the macro to assemble a lens, independent of the feed model, the macro imports a model whose phase centre is in the position $P(x, y, z) = (0,0,0)$, as shown in Figure 14. This way, the macro has to import the data given by the MATLAB application, presented in Figure 11 (b), and the feed (Figure 14), as demonstrated in Figure 15.

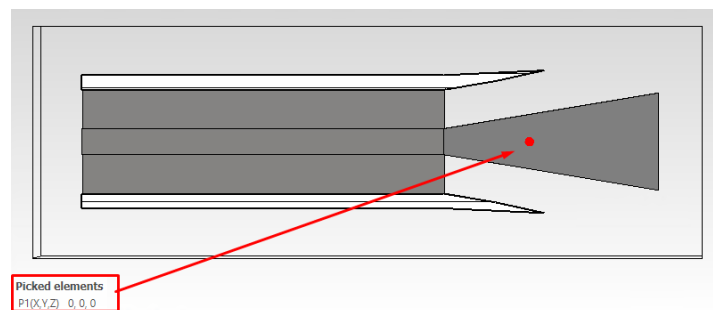


Figure 14: Feed Model.

```
' Rotman Lens

Public Const f1 = 6           'Rotman Lens f1 value
Public Const w1 = 15.7       'Wavelength
Public Const height = 3.4036 'Height of the Lens
Public Const thick = 2       'Metal Thickness
Public Const Nb = 9          'Number of Beam Ports
Public Const Na = 7          'Number of Array Ports
'Public Const CPwg = 11      'Center Point of the Waveguide

'Port positions and angles:
Public Const arraypoints = "D:\Fábio Cardoso\Macro\arraypoints.txt"
Public Const beampoints = "D:\Fábio Cardoso\Macro\beampoints.txt"
Public Const waveguidemodel = "D:\Fábio Cardoso\Macro\waveguidemodel.txt.sab"

Option Explicit

Sub Main ()
```

Figure 15: Macro (Imports) CST – Microwave Studio.

This macro is found in the Attachments section at the end of this thesis.

2.4.2. Full model assembly

This automated process allows us to do quick tests, and in this way evaluate various models. The basic concept is simple and is illustrated in the Figure 16. We start by defining the set of equations in GO that will be applied to the model. After that, the model is implemented into the MATLAB application. From this point, a cycle is formed where we create several models until we are satisfied with the results and discussion of them.

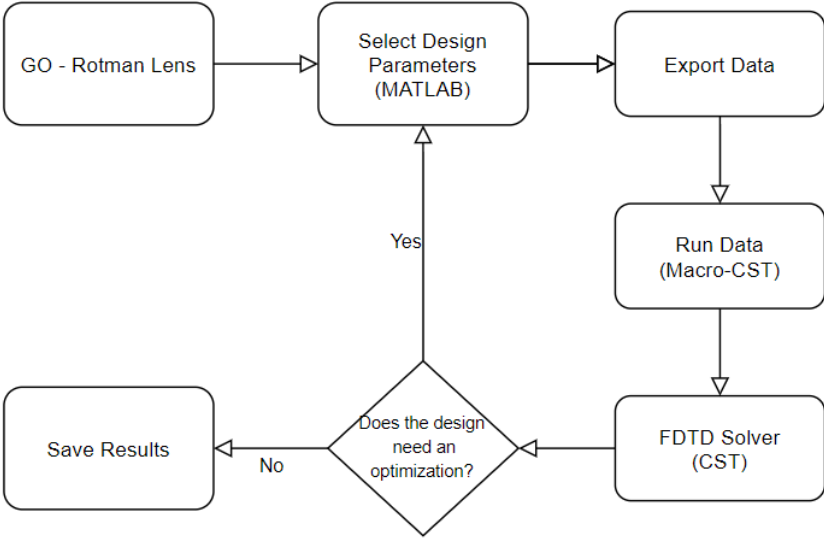


Figure 16: Flowchart of the automated system developed

CHAPTER THREE

Initial Assessment

3.1. Introduction

This chapter is dedicated to the study of a simple Rotman Lens model. Before moving on to a more complex system, an initial evaluation of a simple model is made to test its viability in an attempt to create a starting point for the further development of a more complete model.

The lens presented in this chapter is composed by 5 input and 5 output ports, with a maximum beam scanning of 20° . The connection between the input and output ports is done through a PPW in the TEM regime. This simple configuration allows to have an initial assessment of the antenna port isolation and return losses, for the designed ridge to PPW transitions. This preliminary work shows promising results, which pave the way for future improvements in terms of bandwidth and scanning performance.

This chapter is organized as follows. In Section 3.2., the design of the RL based on GO is shown. In Section 3.3., a full-wave analysis of the ridge waveguide to PPW transition is presented. In Section 3.4., the numerical results for the complete RL are shown. Finally, the conclusions are drawn in Section 3.5..

3.2. Rotman Lens Design

The position of the input and output ports, as well as the size of the TLs, follows the traditional design rule of the lens in [19]. For the design frequency, we have chosen 24.15 GHz, as it represents the centre of the band in study (17.3-31 GHz). The adopted numerical values of the lens are given in Table 1. We used our tool to calculate the position of the input and output ports, and to confirm our calculations we used the software developed by Simon, P. S. [26], resulting in the beam and array contour plotted in Figure 17. As mentioned previously, this is a preliminary test to assess if the adopted ridged waveguide ports and transitions can operate in the intended bandwidth with good port isolation and insertion losses, when placed along the focal arc and inner lens contour.

Table 1. Design parameters for the Rotman Lens

Number of input ports	5
Number of output ports	5
Focal angle, α	$\pm 35^\circ$
Focal ratio, β	1
Maximum beam angle, ψ	$\pm 20^\circ$
Focal length, f_1	6l
Array element spacing, Δd	1.5l

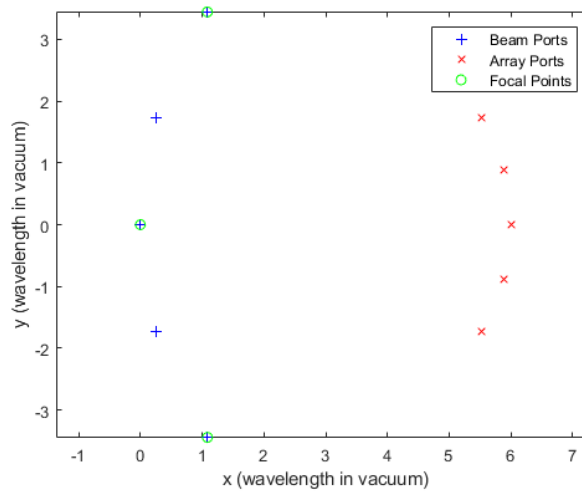


Figure 17: Beam and array contour phase centres [MATLAB], adapted from Simon, P.S. [26]

3.3. Feeding Network

The performance of the antenna will depend on the type of TLs that will connect to the input and output ports, as well as the corresponding transitions. In this chapter, the design used is inspired by the design presented in [8] and adapted to operate in the bandwidth between 17.3 and 31 GHz. Although the feed reported in [8] shows smooth transitions on the lateral, upper and bottom flares, in this chapter we follow an approach resembling [4]. The upper and bottom flares or transitions into the lens have a straight profile. For the lateral flares, the equations used are the same as in [4]. These equations can round off or straighten the lateral flares.

To conclude, the feed design is a scaled-up design, to access the viability of this type of feed in this bandwidth. The feed design is presented in Figure 18.

Table 2. Feed design values

Variable	Value (in mm)
a	6.8
b	3.25
l_1	7
l_2	5
m	1.23
n	1
r_1	4
r_2	7
b_r	1.4

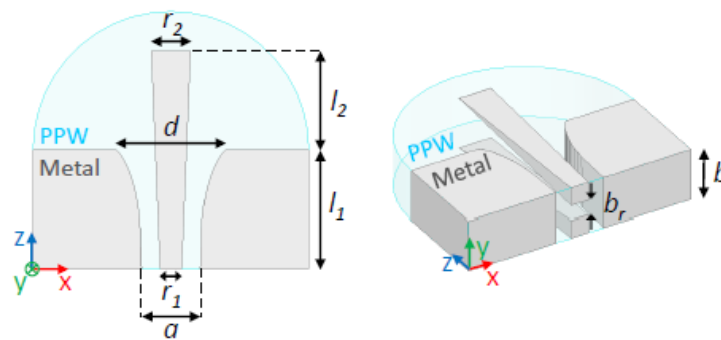


Figure 18: Single Feeding Port (adapted from [4])

Figure 19 and Figure 20 present some tests and results obtained during the creation of this feed. All full wave analyses were made using CST Microwave Studio.

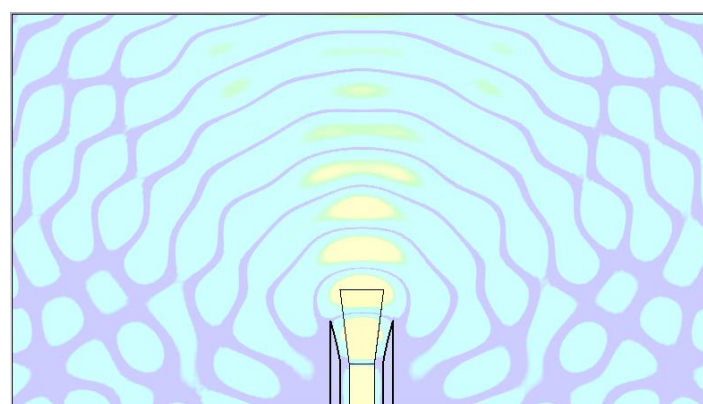


Figure 19: Simulated E-Fields of a single feed at 24.15 GHz

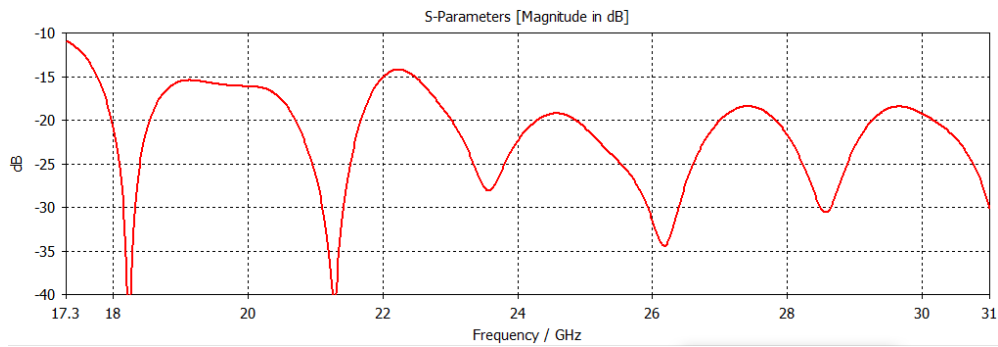


Figure 20: Simulated S11 for a single feed port

As Figure 20 depicts, from 17.3 to 31 GHz, we obtained results below -10 dB. Furthermore, in order to replicate the reflections of a closed surface, that is, a closed beam port contour, we extended the side walls of the feed.

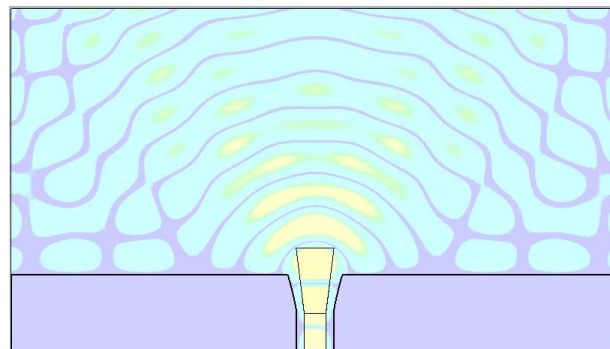


Figure 21: Simulated E-Fields of a single feed with extended side walls at 24.15 GHz

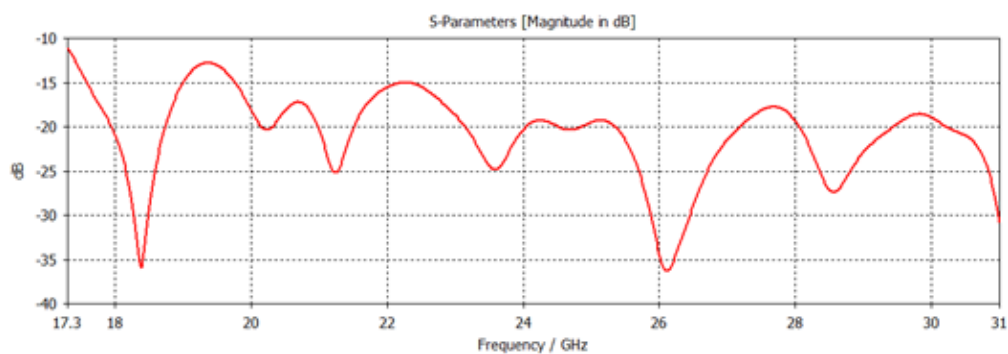


Figure 22: Simulated S11 for a single feed port with extended side walls at 24.15 GHz

Figure 22 shows promising results. It demonstrates that, even with reflections possibly brought by a closed contour, the S11 results still remain below -10 dB.

To evaluate the coupling between adjacent ports, and the transmission of these ports, from BPs to APs, we reproduced a simple model with 3 ports side by side with the lateral sides open. In order to have a more realistic approach, we added 3 feeds inside the PPW distanced by f_1 , to simulate some of the reflections the APs could have on the BPs (Figure 23).

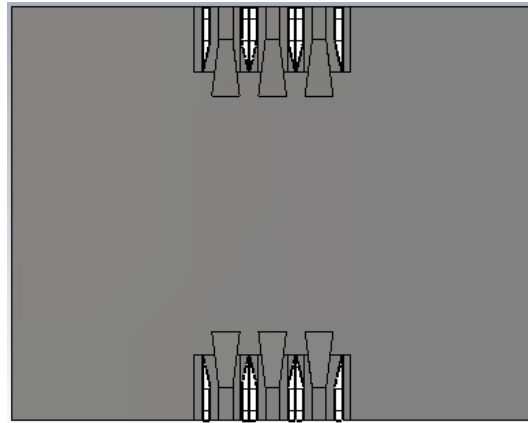


Figure 23: Model to evaluate mutual coupling between adjacent ports. Beam port 1 (left), beam port 2 (middle), and port 3 (right).

In Figure 24, we verify that the isolation between ports is relatively good, since in most of the bandwidth, the S parameters stay below -10 dB. The worst results came from the S11, S22 and S33, at the beginning of the bandwidth with lower frequency values (17.3 to 18GHz). Further improvements can be made to ensure that isolation is below -10 dB from 17.3 GHz to 18 GHz.

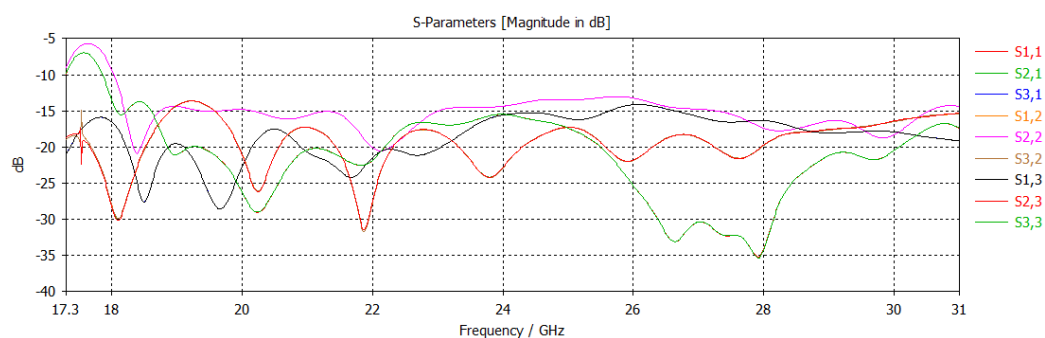


Figure 24: Simulated S parameters of the 3 adjacent feeds

3.4. Rotman Lens Full-Wave Simulation

In this section, we reveal a final design of the lens, with the feeds embedded and rightly positioned. This prototype is a 5x5 lens, as displayed in Figure 25. The final RL design was simulated from 17.3 to 31 GHz and promising results were obtained. The E-Field for 3 beam ports at 17.3, 24.15 and 31 GHz are shown in Figure 25, Figure 26 and Figure 27, respectively. The corresponding S-parameters are shown in Figure 28, Figure 29 and Figure 30, for each beam port.

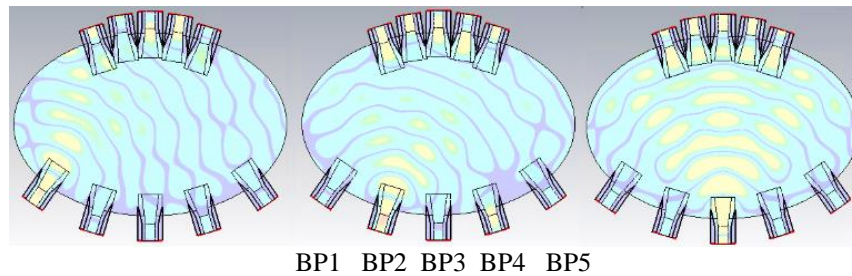


Figure 25: Simulated E-Fields at 17.3 GHz for beam port 1 (left), beam port 2 (middle), and port 3 (right)

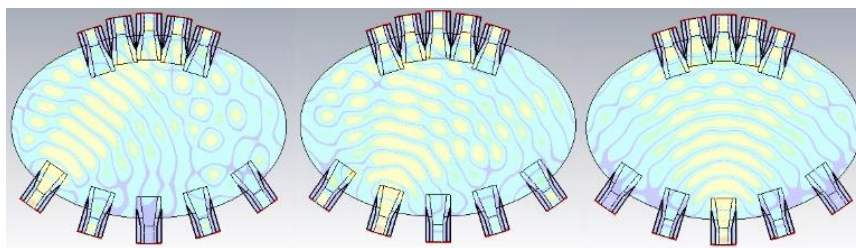


Figure 26: Simulated E-Fields at 24.15 GHz for beam port 1 (left), beam port 2 (middle), and port 3 (right)

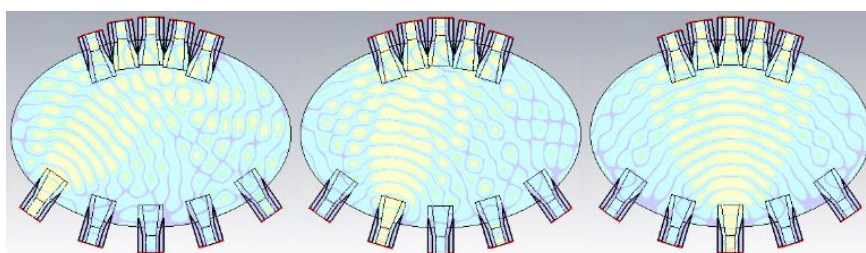


Figure 27: Simulated E-Fields at 31 GHz for beam port 1 (left), beam port 2 (middle), and port 3 (right)

As expected, the end ports, that are the ports from the extremities, present the worst performances (see S11 and S51 in Figure 28). This preliminary study shows that the S-parameters can be below -10 dB in a wide frequency range. However, further optimization must be done to reach the goal of a ultrawideband from 17.3 GHz to 31 GHz. Furthermore, as Figure 22 and Figure 24 suggest, as the feeds are placed closer and in an enclosed system, the coupling between adjacent ports can degrade this response.

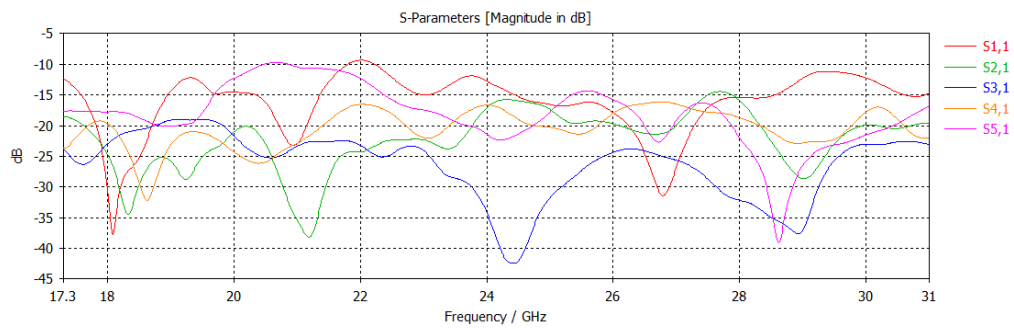


Figure 28: S-parameters from 17.3 to 31 GHz, for Beam Port 1

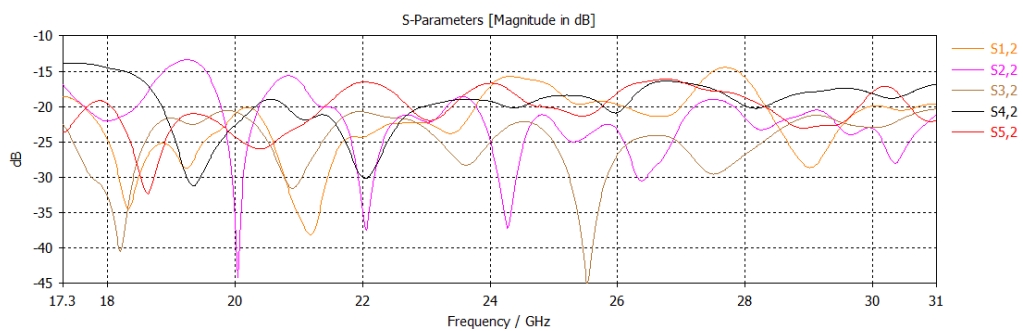


Figure 29: S-parameters from 17.3 to 31 GHz, for Beam Port 2

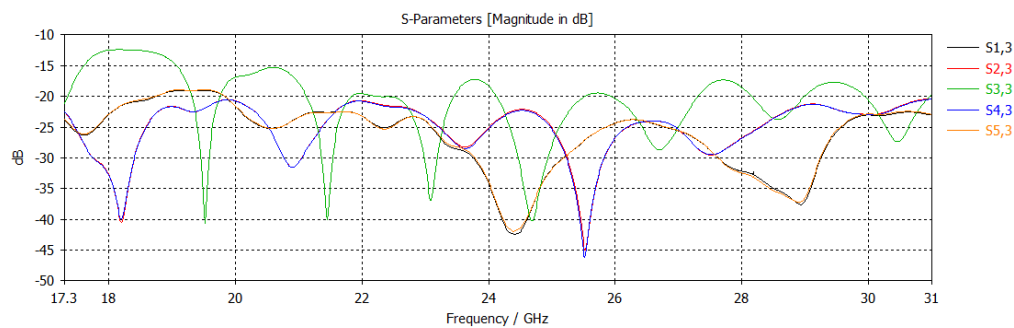


Figure 30: S-parameters from 17.3 to 31 GHz, for Beam Port 3

3.5. Conclusions

This chapter presents a RL lens design based on ridge waveguide technology to operate in the Rx and Tx K/K_a bands of satellite communications. The preliminary design shows promising results. However, further optimization will be required to achieve the entire operating band. The TLs were not added in this part because this was just a test to assess the viability of the transitions between the feed and PPW.

In the following chapter, a standardised double ridge waveguide solution will be explored (WRD 180), in order to take advantage of its bandwidth. The TLs will also be added to complete the design. Since the initial assessment was successful and viable, we will now focus on achieving the next goals of this thesis:

- Create a complete RL;
- Incorporate a larger bandwidth;
- Reduce reflections and phase errors.

CHAPTER FOUR

Rotman Lens Operating in the Full K/K_a Band**4.1. Introduction**

In this section, the final model of this work is presented. As concluded in the previous chapter, there are promising results that can be further explored and improved. Throughout these months, several attempts were made to build a complete lens, resulting in this final design that is now presented. It consists of a 13×7 RL with a scanning range of $\pm 50^\circ$ operating between an ultra-wide band of 16 to 40 GHz, using standard double ridge waveguides (WRD180) with a bandwidth of 18 to 40 GHz as APs and BPs. The results were validated through full-wave simulations.

This Chapter is organized as follows. In Section 4.2., the general design of the RL is shown, as well as the transition design, and some considerations and optimizations are carried out. In Section 4.3. the final assembly of the antenna is presented. In Section 4.4, the numerical results are presented and discussed.

4.2. RL Design**4.2.1. Geometry**

The general design rules of a RL are well established throughout this thesis. GO is applied for the definition of the paths from the BPs, through the APs and ending at the REs (Figure 8). However, the initial values need to be adjusted considering the real structure of the BPs and APs (in this case, the standard ridges WRD180) and corresponding transitions to the PPW. The design parameters are shown in Table 3. These values followed from an iterative optimization using preliminary full-wave tests, as it will be discussed in section 4.2.3. We limited the number of ports to keep the associated computational effort manageable, which is required for full-wave optimizations. A practical design may be adapted in size to meet given requirements. The focal length f_1 was kept as low as possible, ensuring low reflections and good illuminations of the APs, according to full-wave results. The value of β , that controls the shape of the focal arc, was adjusted to minimize the coupling between adjacent ports. The profile of the focal arc and inner lens contour are shown in Figure 31.

Table 3 – Design parameter of the Rotman Lens

Variable	Value
Number of input ports	13
Number of output ports	7
Focal angle, α	$\pm 27^\circ$
Focal ratio, $\beta = f_2/f_1$	0.97
Maximum beam angle, ψ_{\max}	$\pm 50^\circ$
Focal length, f_1 (mm)	137
Array element spacing, Δd (mm)	9.7

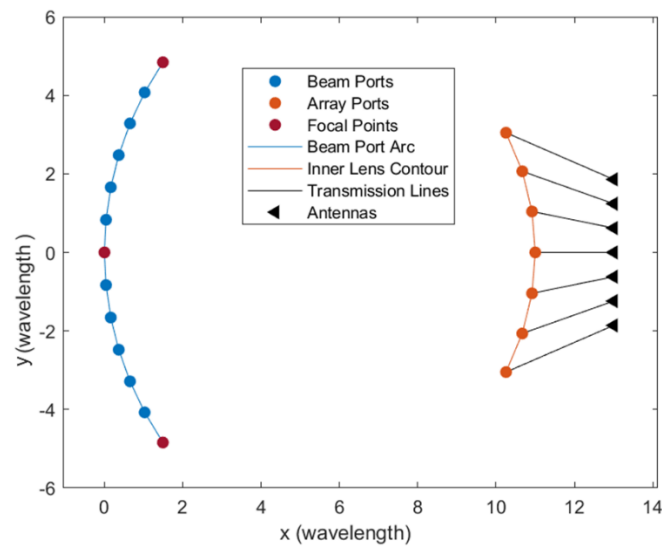


Figure 31: Profile of the designed Rotman Lens.

4.2.2. Double Ridge Waveguide to PPW Transition

In the previous chapter, we used a personalized feed, whilst in the present chapter it is used a standard waveguide (WRD180). A proper design of a transition is required to ensure a wideband behaviour of the lens. The design proposed in [4] was adapted and optimized to operate between 16 and 40 GHz. The final dimensions are shown in Figure 32, which also contains a representation of the positioning of these transitions along the focal arc, illustrating a cavity introduced between adjacent ports (Figure 32 (b)).

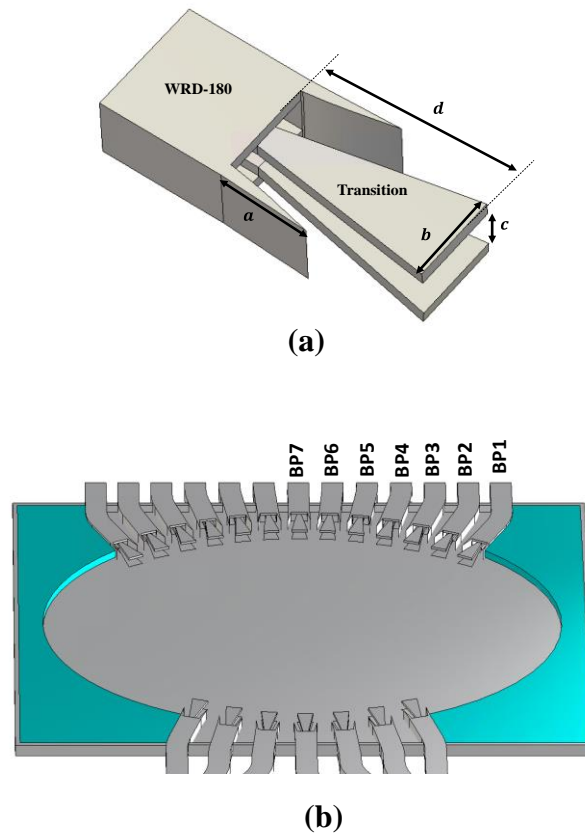


Figure 32: (a) Geometry of the design Ridge to PPW transitions with $a = 7 \text{ mm}$, $b = 6.8 \text{ mm}$, $c = 3.4 \text{ mm}$, $d = 14.9 \text{ mm}$. (b) Transitions in the Rotman lens.

4.2.3. Considerations and optimizations

During the elaboration of this model, there have been several modifications that affected the antenna's performance. Here, some of these changes are demonstrated, justifying some of the decisions made in the lens design.

One of the initial designs was filled with absorbent in between each port, as shown in Figure 33. One of our studies showed that there exists a trade-off by removing and adding this absorbent. With the absorbent we improve the return losses and coupling but we lose power in process. Nevertheless, we chose to remove the absorbent, since it simplifies the design and assembly, and the return losses were still below the -10 dB mark.

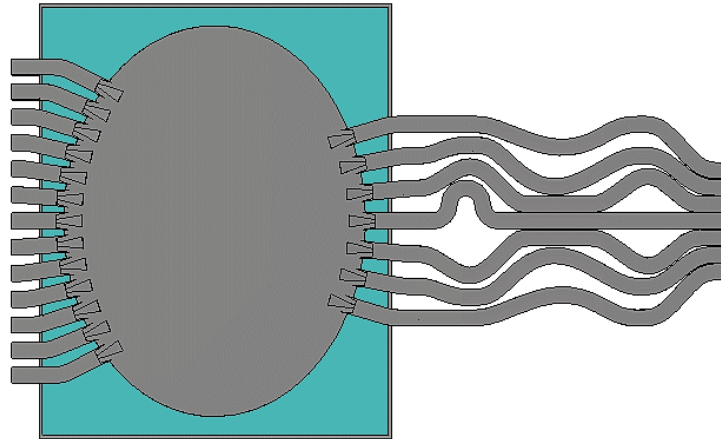


Figure 33: RL with absorber filled, in between each port.

Another adjustment was the value of β . By having a value of $\beta = 1$, the BPs were equally spaced in a circular setup with the centre in f_1 , so none of them was coming more to the front than the others. This did not happen to the APs, so by having them in a more elliptical setup, some were more to the front than others. This had the effect of decreasing the S-Parameters of the APs. To solve this problem, we had to adjust the value of β and bring it to the value of $\beta = 0.97$. By doing this, the BPs had a more elliptical shape and the APs a more circular shape. From that, a new trade-off occurs. By adjusting the value of β , we improve the S-Parameters of the APs, but also decrease the performance of the BPs, as illustrated in Figure 34 and Figure 35.

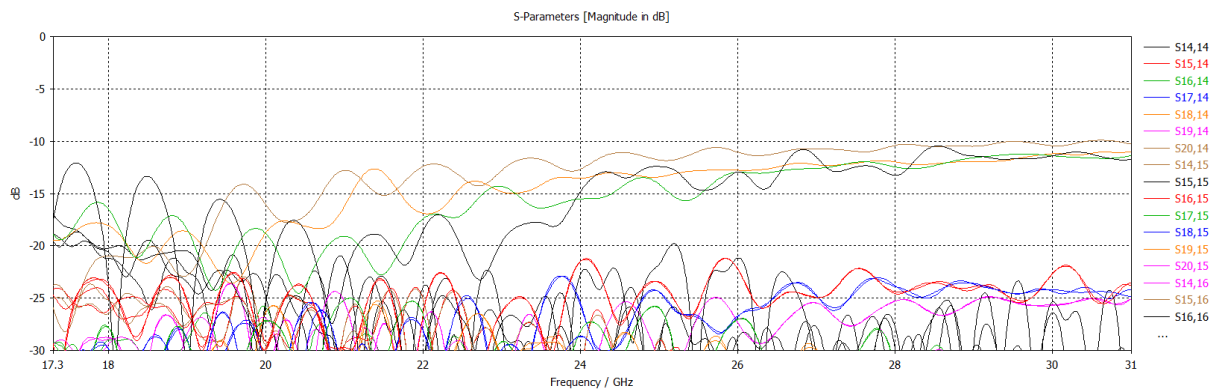


Figure 34: S-Parameters of the APs with $\beta = 1$

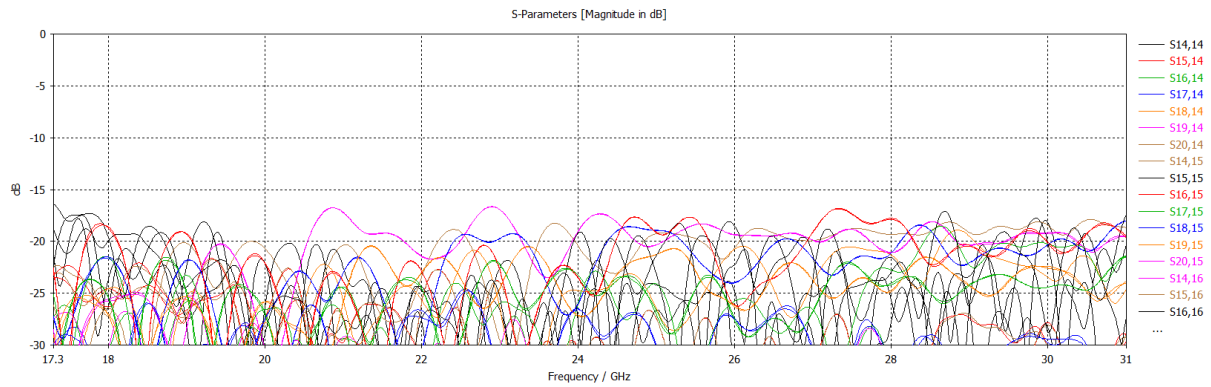


Figure 35: S-Parameters of the APs with $\beta = 0.97$

4.3. Assembling of the Rotman Lens

After positioning all the lens components in the previously calculated locations, the lens is closed. The PPW takes a rectangular shape filled with absorbing material (ECCOSORB NA 77) on the sides, so that reflections due to spill over are minimized. The absorbing material on the sides of the cavity can be removed, by adding new ports (including dummy ports) which would allow achieving an all-metal design. Finally, the TLs, designed using Bézier curves, are added, completing the RL beamformer. Figure 36 shows the final design of the lens.

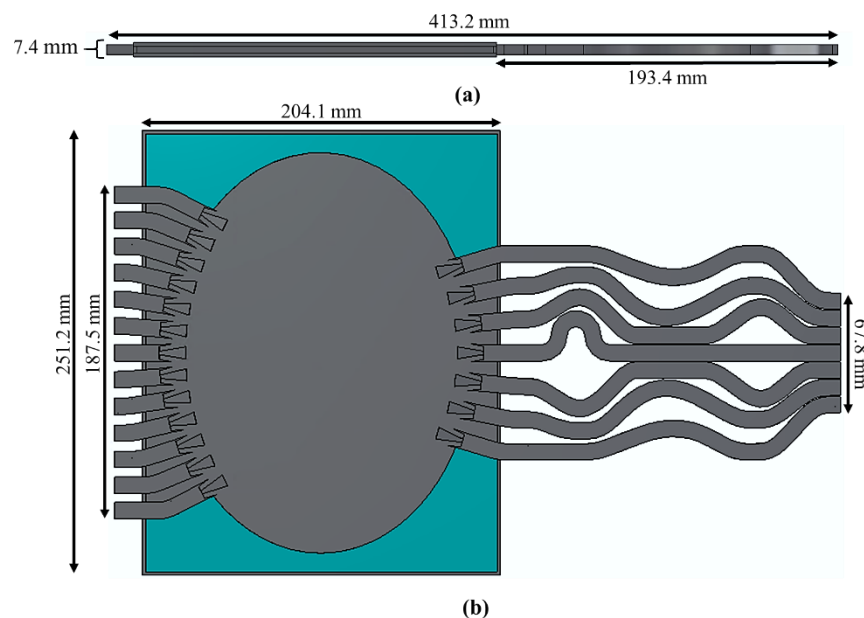


Figure 36: 3D Model representation [CST]: (a) side view; (b) top view

4.4. Numerical results and discussion

This section shows the full-wave simulation results of the model presented in Figure 36. The model was simulated from 16 to 40 GHz using the FDTD solver of CST Microwave Studio. In Figure 39 it is shown that all the scattering parameters between the BPs are well below -10 dB over the entire analysed band, as well as the APs (Figure 40).

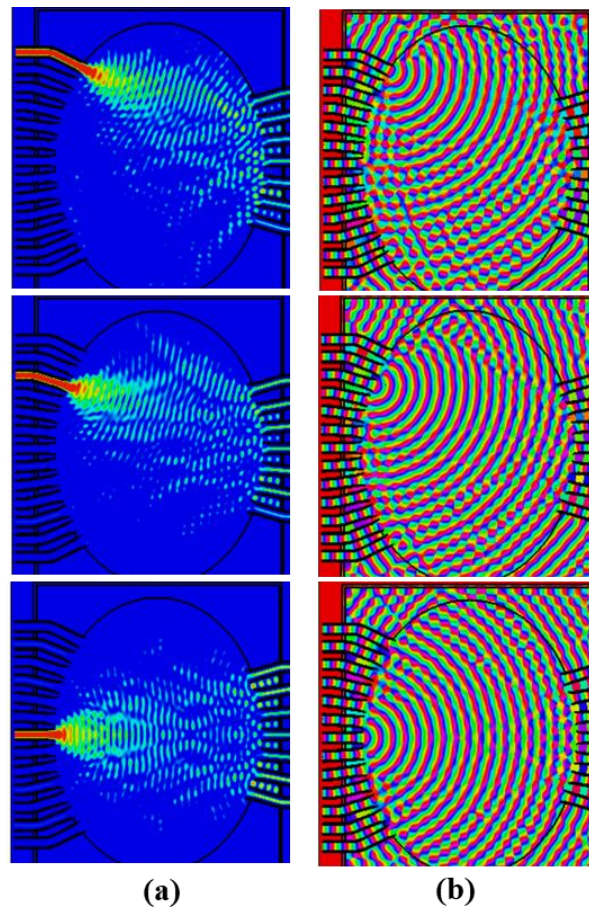


Figure 37: Amplitude (a) and phase (b) field distribution inside RL for 30 GHz for three different beam port excitations.

From Figure 37 we can see that not all the APs receive the same amount of energy. This results in a different field magnitude for each AP, which decreases the performance of the array factor. From Figure 38, we can see that in lower frequencies we achieve a better harmonization of the Field magnitude across all APs. This harmonization is worse in higher frequencies, like 40 GHz.

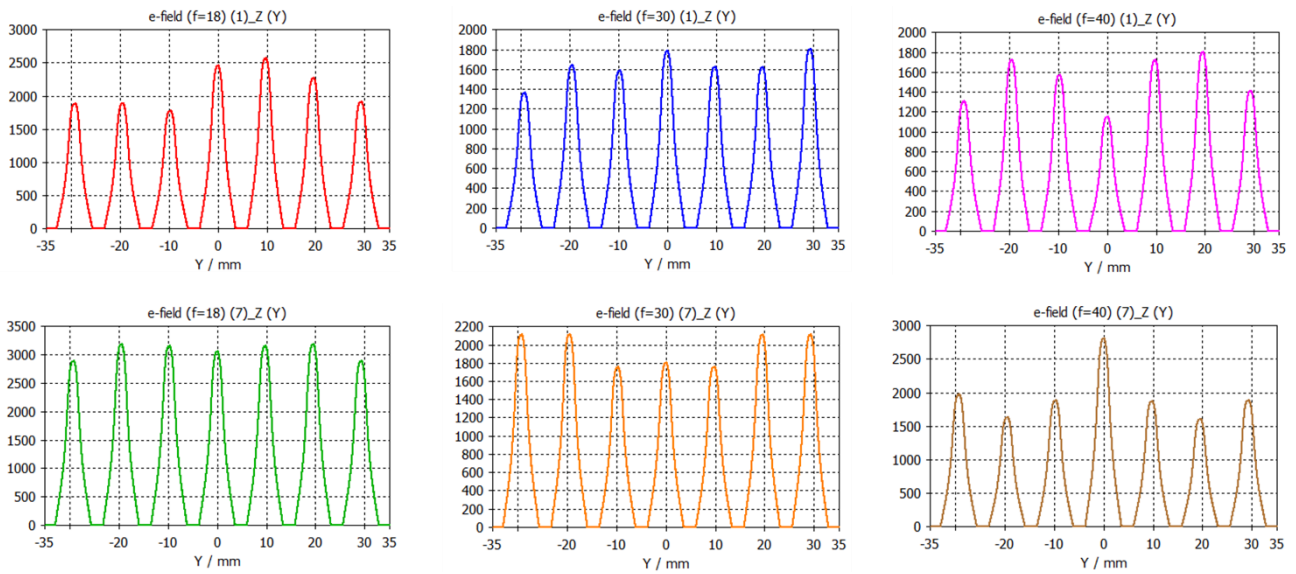


Figure 38: Field magnitude distribution. Top row represents BP1 and lower row BP7 (Centre)

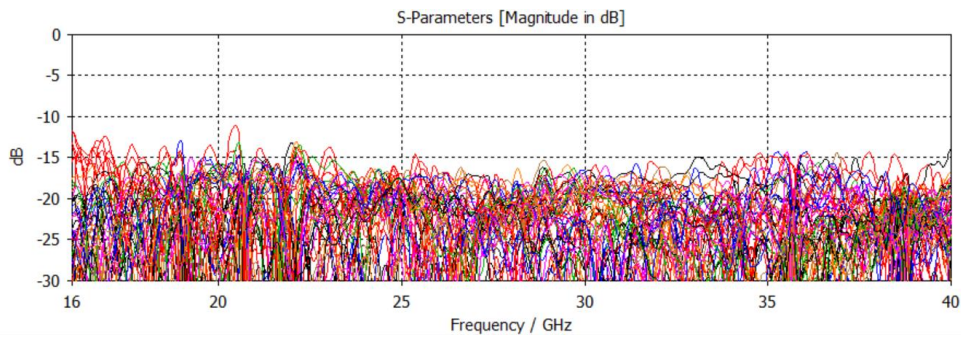


Figure 39: S-parameters between all beam ports 16 to 40 GHz.

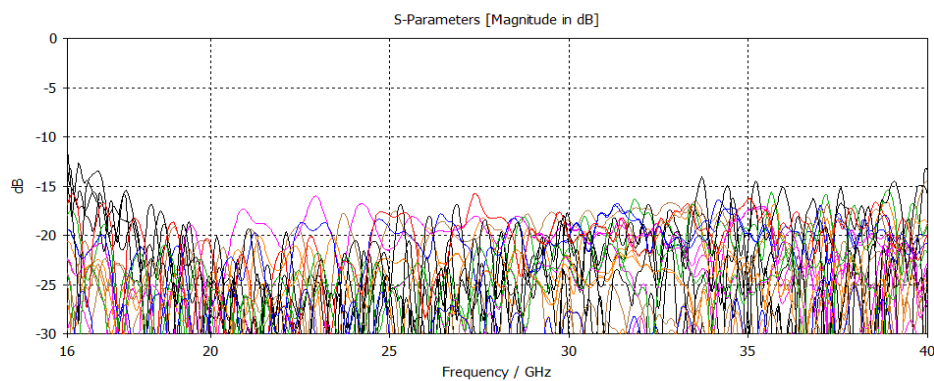


Figure 40: S-parameters between all array ports 16 to 40 GHz.

The field amplitude and phase representation inside the lens, for different beam ports at 30 GHz, is shown in Figure 37. This representation highlights the role of the cavities between the APs on reducing reflections back to the BPs. As expected, due to the small size of the inner lens contour, a significant spill over is observed. This may be mitigated by adding more APs. However, this would increase the numerical complexity of the analysis. The presented design is sufficient for showing the broadband potential of this approach.

Figure 41 shows the phase variation at the output of the TLs for two beam positions, the central one and the most scanned one, confirming the stable design of the complete beamformer over the analysed frequency range. In Table 4, the beam direction and corresponding phase errors are also presented. The corresponding array factors for port 1, 3 and 7 for 18 and 30 GHz are represented in Figure 42. A good agreement of the full-wave results with the reference case of ideal linear phase variation and constant amplitude is obtained. We have chosen only three ports because in some cases the secondary lobe emerges, and since we have a good number of ports this can result in a confusing analysis for the reader. With that being said, we have chosen the port with the highest beam tilt (Port 1), the centre port (Port 7) and one in between (Port 3).

Table 4 - Beam direction and average phase error for sequential beam port excitation (see Figure 32 (b)), at 18 GHz, 30 GHz, 40 GHz.

BP (#)	18 GHZ		30 GHZ		40 GHZ	
	ψ (°)	Average Error (°)	ψ (°)	Average Error (°)	ψ (°)	Average Error (°)
1	50.6	7.1	48.9	12.0	49.0	19.9
2	40.2	9.8	39.9	10.0	39.1	19.7
3	30.8	5.6	30.7	11.2	30.1	13.6
4	23.0	9.5	22.6	15.0	22.0	19.7
5	14.9	9.8	14.0	12.7	14.3	28.0
6	7.7	9.3	7.5	15.7	7.0	20.8
7	0.0	10.2	0.0	7.0	0.0	18.5

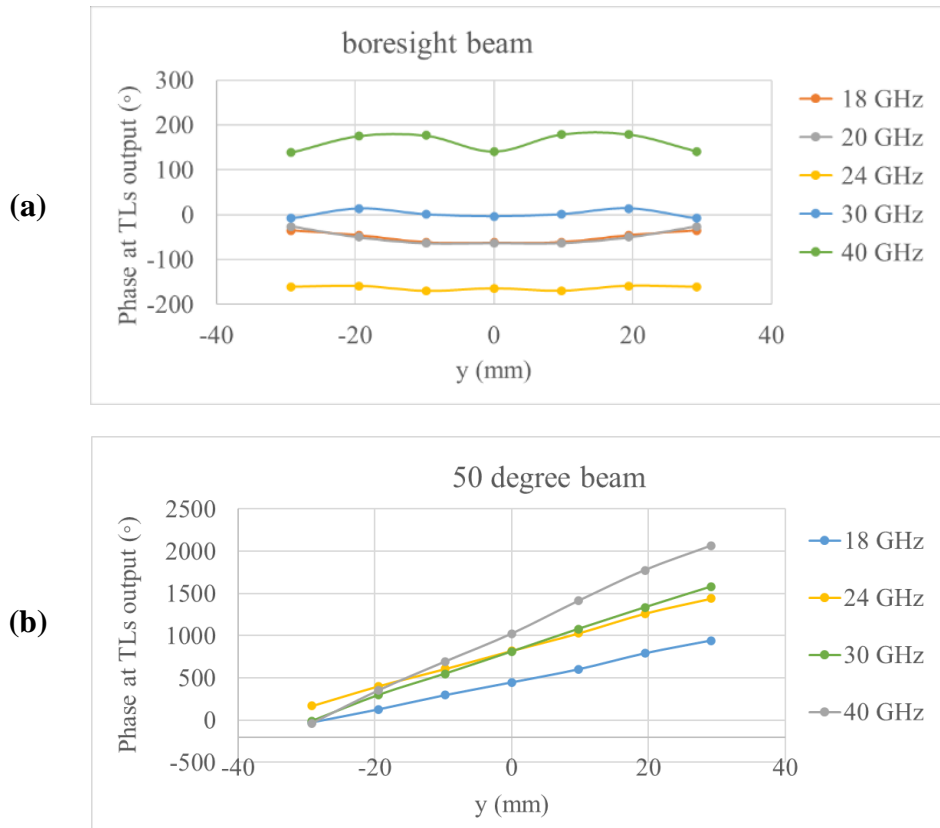


Figure 41: Phase at the output ports of the TLs (each dot corresponds to a different TL) considering multiple frequencies for the central port (a) and most scanned one (b).

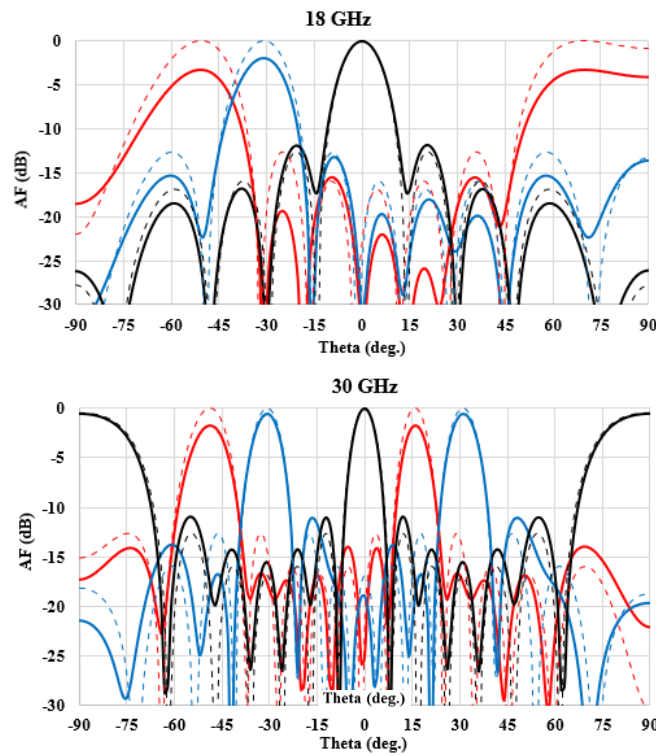


Figure 42: Array factors for ports 1,3 and 7 at 18 GHz and 30 GHz. Comparison of the full-wave simulations (solid lines) with the case of ideal linear phase variations and constant amplitude (dashed lines).

Finally, we decided to evaluate the antenna’s power efficiency. We have chosen BP1 and BP7, as they represent the BPs with the worst and best performance, respectively. As Figure 43 illustrates, there are some frequencies where the antenna’s efficiency decreases. This is notorious in the central BP (BP7), where around 19GHz this effect occurs. For the BP1, the efficiency is stable but is still in need of improvement for future work.

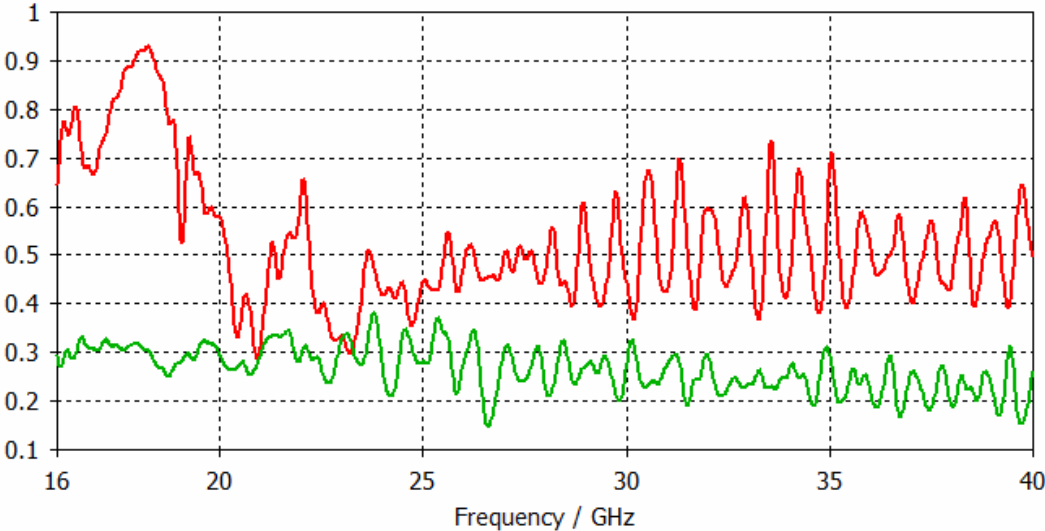


Figure 43: Antenna power efficiency. Green line represents Beam Port 1(Extremity), and the red line represents Beam Port 7 (Centre)

CHAPTER FIVE

Conclusions

5.1. *Main achievements*

In this Thesis, a novel transition design of a double ridged waveguide in a parallel plate waveguide, in the context of a Rotman Lens antenna, is proposed. We achieved an ultrawide band operation (16-40 GHz), exploiting the bandwidth potential of the WRD180.

The challenge was to find cost-effective solutions for broadband antennas, capable of performing multibeam and/or wide beam scanning. The qualities of the Rotman Lens were explored to the uttermost, to face this major challenge. Nevertheless, this classical antenna presents a complex assembly, with several independently designed parts. All these components had to be carefully positioned in previously calculated points, always paying attention to overlapping situations. For this, we relied in automated processes, like macros (CST – Microwave Studio), and applications (MATLAB).

In this work, we not only assessed the viability of this type of feed (Double Ridged Waveguide) in the K/K_a Bands, but also have reached all of the listed objectives in Chapter One. Our initial objective was to operate in the entire K/K_a satellite Band (17.3 GHz-31GHz) [37], but we were able to extend it further to 16-40 GHz. Good performance indicators of our lens were shown in Chapter Four. Not only the scattering parameters between the beam ports and array ports were well below – 10 dB, but the phase was frequency independent, with larger errors in higher frequencies. This demonstrated that the Rotman Lens designed was indeed functioning well. The field distribution along the APs is one of the topics to improve, as well as the secondary sidelobes levels and the antenna's power efficiency.

We also concluded that, in building this structure (RL), there exists several trade-offs to consider for future work:

1. A cavity is implemented between each feeding ports, which has a positive impact on the return loss and port-to-port coupling at the expense of a moderate increase in the distance between adjacent ports.
2. The value of β can be adjusted to improve the S-Parameters of the APs, at the expense of decreasing the performance of the BPs' S-Parameters.
3. Adding absorbent material in between ports causes the system to lose power, but removing it increases the oscillations of the transmission coefficients, increasing the return losses and coupling.

Finally, in Table 5, the presented design is compared with other published broadband RL designs in terms of lens size, TL technology, scanning range, frequency range and 10 dB return loss bandwidth. This comparison clearly highlights the benefits of the presented design.

Table 5 - Comparing different broadband Rotman lens designs.

	Size	Tech.	Scan	Freq. (GHz)	10 dB Bandwidth
[4]	13×11	Ridge	±15 °	37-43	15%
[9]	5×5	Ridge	±30 °	6-18	100%
[40]	18×16	Microstrip + PMU	±30° RL ±60° RL+PMU	20-25	23%
This work	13×7	Ridge	±50 °	16-40	86%

At the end, our all-metal approach had to have the addition of an absorbent material, because of the reflections in an enclosed system. Ultimately, we are happy to pave the way for future work on this classical antenna, Rotman Lens.

5.2. Future work

There is still a lot of room for improvement in this project. Future works will include investigation on the design of the proposed cavities, ways to remove the absorbent material and create a fully metalized structure, and the creation of radiating elements able to operate in all the band we achieved in the proposed design (16-40 GHz). There are still micro-optimizations to be done, namely the spacing between the feeds, lens size and some other approaches to be implemented, stated in the state of the art, as well as experimental validation.

It would be interesting to also explore the addition of extra components, like phase management units [40] or even polarizers [36], and modify the feed structure to work with power dividers [30].

References

- [1] “Space for 5G | ESA’s ARTES Programmes.” <https://artes.esa.int/space-5g> (accessed Nov. 26, 2020).
- [2] P. Angeletti and M. Lisi, “Multimode beamforming networks for space applications,” *IEEE Antennas Propag. Mag.*, vol. 56, no. 1, pp. 62–78, 2014, doi: 10.1109/MAP.2014.6821760.
- [3] S. Vashist, M. K. Soni, and P. K. Singhal, “A Review on the Development of Rotman Lens Antenna,” *Chinese J. Eng.*, vol. 2014, pp. 1–9, 2014, doi: 10.1155/2014/385385.
- [4] S. A. Gomanne, N. J. G. Fonseca, P. Jankovic, J. Galdeano, G. Toso, and P. Angeletti, “Rotman Lenses with Ridged Waveguides in Q-Band,” *14th Eur. Conf. Antennas Propagation, EuCAP 2020*, 2020, doi: 10.23919/EuCAP48036.2020.9135218.
- [5] W. E. Kock, “Metal-Lens Antennas,” *Proc. IRE*, vol. 34, no. 11, pp. 828–836, Nov. 1946, doi: 10.1109/JRPROC.1946.232264.
- [6] J. Ruze, “Wide-Angle Metal-Plate Optics,” *Proc. IRE*, vol. 38, no. 1, pp. 53–59, 1950, doi: 10.1109/JRPROC.1950.232789.
- [7] W. Rotman and R. F. Turner, “Wide-Angle Microwave Lens for Line Source Applications,” *IEEE Trans. Antennas Propag.*, vol. 11, no. 6, pp. 623–632, 1963, doi: 10.1109/TAP.1963.1138114.
- [8] P. Knott, “Design of a ridged waveguide feed network for a wideband rotman lens antenna array,” *2008 IEEE Radar Conference, RADAR 2008*. 2008, doi: 10.1109/RADAR.2008.4720857.
- [9] K. V. Hoel, S. Kristoffersen, N. Jastram, and D. S. Filipovic, “3D printed Rotman lens,” *Eur. Microw. Week 2017 “A Prime Year a Prime Event”, EuMW 2017 - Conf. Proceedings; 47th Eur. Microw. Conf. EuMC 2017*, vol. 2017-Janua, pp. 125–128, Oct. 2017, doi: 10.23919/EuMC.2017.8230815.
- [10] S. A. Gomanne, N. J. G. Fonseca, P. Jankovic, G. Toso, and P. Angeletti, “Comparative Study of Waveguide Rotman Lens Designs for Q/V Band Applications,” *40th ESA Antenna Work. Dev. Terr. Small Sp. Platforms*, no. October, pp. 1–8, 2019.
- [11] D. R. Gagnon, “Procedure for correct refocusing of the Rotman lens according to Snell’s law,” *IEEE Trans. Antennas Propag.*, vol. 37, no. 3, pp. 390–392, Mar. 1989, doi: 10.1109/8.18736.
- [12] R. C. Hansen, *Phased Array Antennas*, Second. Hoboken, NJ, USA: John Wiley &

- Sons, Inc., 2009.
- [13] J. Dong, A. I. Zaghloul, and R. Rotman, "Phase-error performance of multi-focal and non-focal two-dimensional Rotman lens designs," *IET Microwaves, Antennas Propag.*, vol. 4, no. 12, pp. 2097–2103, 2010, doi: 10.1049/iet-map.2009.0565.
- [14] J. Shelton, "Focusing characteristics of symmetrically configured bootlace lenses," *IEEE Trans. Antennas Propag.*, vol. 26, no. 4, pp. 513–518, Jul. 1978, doi: 10.1109/TAP.1978.1141883.
- [15] M. Maybell, "Ray structure method for coupling coefficient analysis of the two dimensional Rotman lens," in *1981 Antennas and Propagation Society International Symposium*, 1981, vol. 19, no. 5, pp. 144–147, doi: 10.1109/APS.1981.1148557.
- [16] T. Katagi, S. Mano, and S. Sato, "An improved design method of Rotman lens antennas," *IEEE Trans. Antennas Propag.*, vol. 32, no. 5, pp. 524–527, May 1984, doi: 10.1109/TAP.1984.1143353.
- [17] L. Musa and M. S. Smith, "Microstrip port design and sidewall absorption for printed rotman lenses," *IEE Proc. H (Microwaves, Antennas Propagation)*, vol. 136, no. 1, pp. 53–58, Feb. 1989, doi: 10.1049/ip-h-2.1989.0009.
- [18] S. Smith, A. K. S. K. S. Fong, M. S. Smith, and A. K. S. K. S. Fong, "Amplitude performance of Ruze and Rotman lenses," *Radio Electron. Eng.*, vol. 53, no. 9, p. 329, Feb. 1983, doi: 10.1049/ree.1983.0061.
- [19] R. C. Hansen, "Design trades for Rotman lenses," *IEEE Trans. Antennas Propag.*, vol. 39, no. 4, pp. 464–472, Apr. 1991, doi: 10.1109/8.81458.
- [20] L. T. Hall, H. J. Hansen, and D. Abbott, "Rotman lens for mm-wavelengths," *Smart Struct. Devices, Syst.*, vol. 4935, p. 215, 2002, doi: 10.1117/12.469727.
- [21] E. O. Rausch and A. F. Peterson, "Rotman lens design issues," in *2005 IEEE Antennas and Propagation Society International Symposium*, 1990, vol. 2B, pp. 35–38, doi: 10.1109/APS.2005.1551928.
- [22] S. Smith, A. K. S. K. S. Fong, M. S. Smith, and A. K. S. K. S. Fong, "Amplitude performance of Ruze and Rotman lenses," *Radio Electron. Eng.*, vol. 53, no. 9, p. 329, Feb. 1983, doi: 10.1049/ree.1983.0061.
- [23] R. Uyuguroglu and A. Y. Oztoprak, "A method for minimizing the phase errors of rotman lenses," *ELECO 2009 - 6th Int. Conf. Electr. Electron. Eng.*, vol. 0, no. 1, pp. 174–176, 2009.
- [24] N. J. G. Fonseca, "A focal curve design method for rotman lenses with wider angular scanning range," *IEEE Antennas Wirel. Propag. Lett.*, vol. 16, no. c, pp. 54–57, 2017,

- doi: 10.1109/LAWP.2016.2554281.
- [25] N. J. G. Fonseca, “An improved design method for two-dimensional Rotman lenses with reduced phase-aberrations,” *IEEE Antennas Propag. Soc. AP-S Int. Symp.*, pp. 1166–1167, 2013, doi: 10.1109/APS.2013.6711243.
- [26] P. S. Simon, “Analysis and synthesis of Rotman lenses,” *A Collect. 22nd AIAA Int. Commun. Satell. Syst. Conf. Exhib. Tech. Pap.*, vol. 2, no. May, pp. 738–748, 2004, doi: 10.2514/6.2004-3196.
- [27] F. C. Suarez, D. N. Mendez, and M. Baquero-Escudero, “Rotman lens with Ridge Gap Waveguide technology for millimeter wave applications,” *2013 7th Eur. Conf. Antennas Propagation, EuCAP 2013*, pp. 4006–4009, 2013.
- [28] J. J. Shea, “Ridge waveguides and passive microwave components [Book Reviews],” *IEEE Electr. Insul. Mag.*, vol. 17, no. 6, pp. 63–63, Nov. 2001, doi: 10.1109/MEI.2001.969948.
- [29] A. Boni, R. Parodi, G. Gemme, A. Gallo, and F. Caspers, “A broadband waveguide to coaxial transition for high order mode damping in particle accelerator rf cavities,” *Part. Accel.*, vol. 45, no. LNF-93-075-P, pp. 195–208, 1993, doi: 10.15161/oar.it/1448897342.82.
- [30] A. F. Peterson, S. Member, and E. O. Rausch, “Scattering Matrix Integral Equation Analysis for the Design of a Waveguide Rotman Lens,” vol. 47, no. 5, pp. 870–878, 1999.
- [31] H.-H. Fuchs and D. Nüßler, “Design of Rotman lens for beamsteering of 94 GHz antenna array,” *Electron. Lett.*, vol. 35, no. 11, p. 854, 1999, doi: 10.1049/el:19990640.
- [32] E. O. Rausch, A. F. Peterson, and W. Wiebach, “Millimeter wave Rotman lens,” *IEEE Natl. Radar Conf. - Proc.*, pp. 78–81, 1997, doi: 10.1109/nrc.1997.588162.
- [33] H. Legay *et al.*, “Multiple beam antenna based on a parallel plate waveguide continuous delay lens beamformer,” *ISAP 2016 - Int. Symp. Antennas Propag.*, pp. 118–119, 2017.
- [34] F. Doucet, N. J. G. Fonseca, E. Girard, H. Legay, and R. Sauleau, “Analytical Model and Study of Continuous Parallel Plate Waveguide Lens-like Multiple-Beam Antennas,” *IEEE Trans. Antennas Propag.*, vol. 66, no. 9, pp. 4426–4436, 2018, doi: 10.1109/TAP.2018.2846768.
- [35] N. J. G. Fonseca *et al.*, “Shaped Continuous Parallel Plate Waveguide Delay Lens-Like Beamformers for Future High Performance Multiple Beam Space,” no. October, pp. 3–8, 2018.

- [36] N. Bartolomei *et al.*, “Circularly Polarized Parallel Plate Waveguide Multiple-Beam Lens-like Antenna for Satcom Applications,” *13th Eur. Conf. Antennas Propagation, EuCAP 2019*, no. EuCAP, pp. 2019–2021, 2019.
- [37] J. Christensen, “ITU regulations for Ka-band satellite networks,” *30th AIAA Int. Commun. Satell. Syst. Conf. (ICSSC), 2012*, pp. 1–8, 2012, doi: 10.2514/6.2012-15179.
- [38] F. Cardoso, S. A. Matos, J. R. Costa, and C. A. Fernandes, “Design of an all-metal broadband Rotman lens for satellite communications at K/Ka-Band,” *2021 Telecoms Conf. ConfTELE 2021*, pp. 8–11, 2021, doi: 10.1109/ConfTELE50222.2021.9435483.
- [39] M. Davis and P. Simon, “SPACE SYSTEMS / LORAL - Formulas for Rotman Lens Design,” 2002.
- [40] E. Tolin, O. Litschke, S. Bruni, and F. Vipiana, “Compact Extended Scan Range Antenna Array Based on Rotman Lens,” *IEEE Trans. Antennas Propag.*, vol. 67, no. 12, pp. 7356–7367, 2019, doi: 10.1109/TAP.2019.2935086.



Attachments

A. *Manual MATLAB Application*

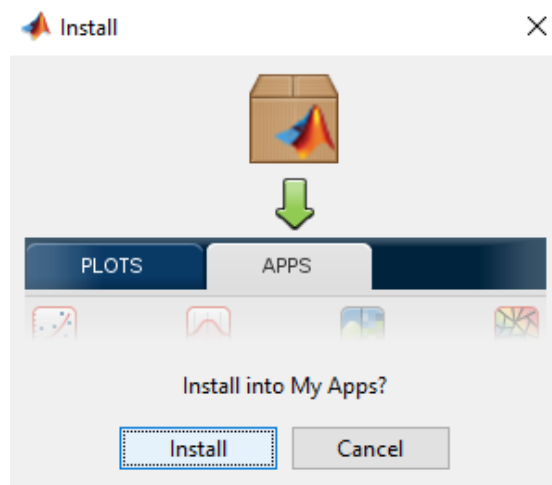
Installation

The installation is pretty simple when using MATLAB applications. The developer shares the package, and the other person needs to follow these rules:

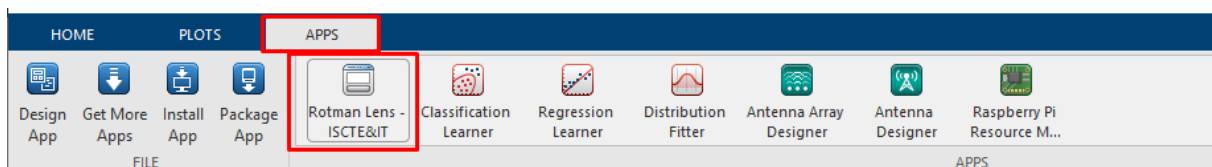
1. Create a Paste for the MATLAB APP to run and save files

Name	Status	Date modified	Type	Size
 Rotman Lens - ISCTE&IT	 R	25/10/2021 16:48	MATLAB App Inst...	259 KB

2. Double click the package and click “Install”



3. In your APPS Tab you should have the program ready to run.



4. Have fun!

GUI

In order to organize the several sections of the GUI, we numbered each section to ease the comprehension of the application (Figure A1).

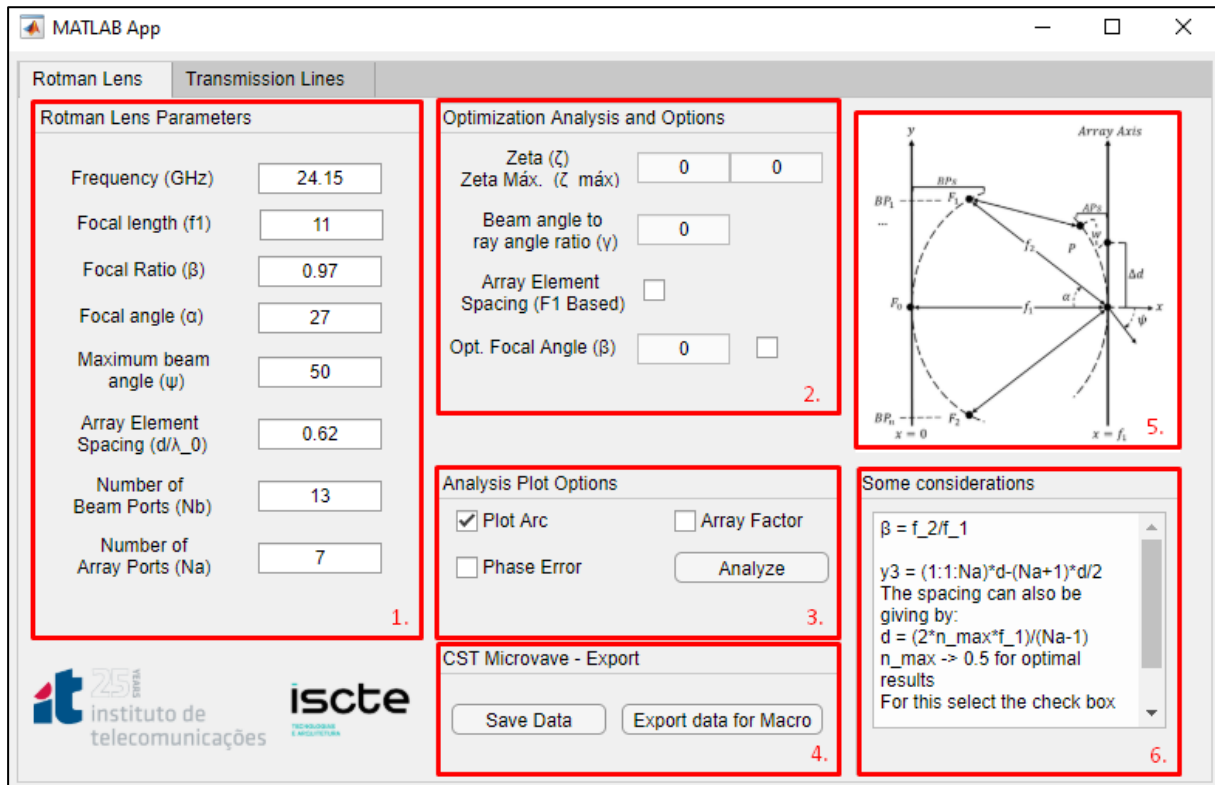


Figure A1: GUI – MATLAB Application

Section 1:

In this Section, we have a set of parameters to design the Rotman Lens antenna.

Section 2:

In this Section, we have some design parameters that can be used to further optimizations by checking the charts obtained from Hansen studies.

Section 3:

In this Section, we have an analysis plot area that enables us to plot the several studies in display.

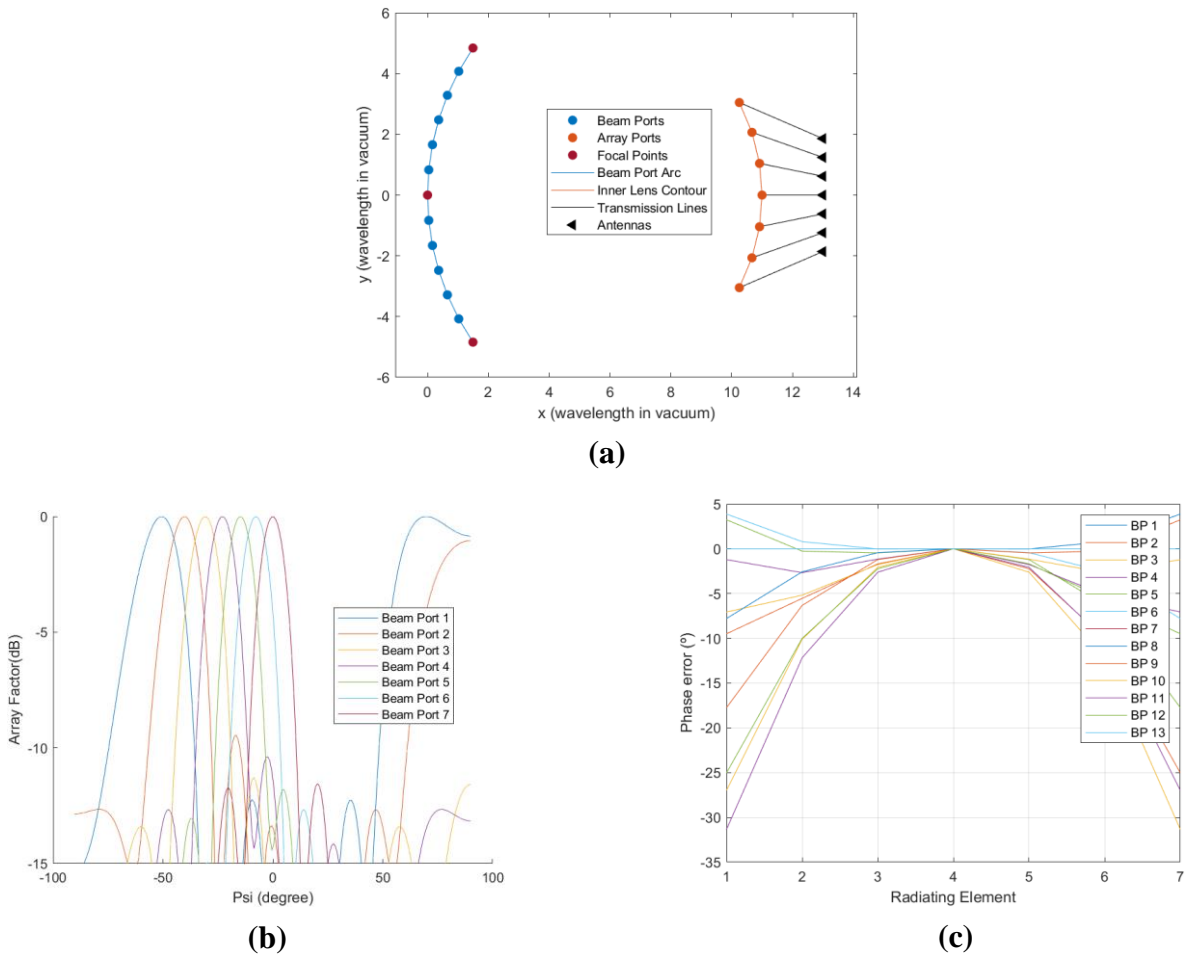


Figure A2: (a) Plot Arc; (b) Array Factor; (c) Phase Error.

Section 4:

In this Section, we have the export area that enables the program to export the results of the analysed design. The “Save Data” button allows the user to save the structure of the previous calculated/analysed Rotman Lens. The “Export data for Macro” button allows the data to be exported and saved in *.txt* files, as shown in Figure A3 and Figure A4. These files can later on be imported by the CST Macro system (Figure A5).

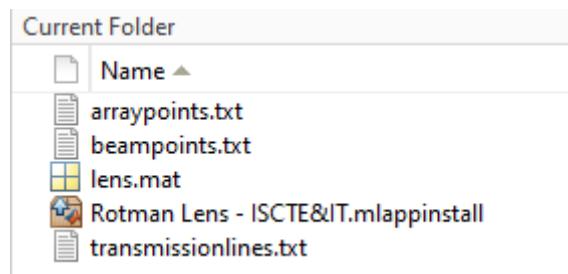


Figure A3: Exporting port positions into the *.txt* files

```

Xb Yb angleb
1.49296038691012 -4.84407863222096 -27
1.02665869693418 -4.07613690255669 -22.229993608725
0.652123873158525 -3.28601050601004 -17.617459181453
0.364772484005884 -2.47885447851159 -13.1202338257239
0.161495976000238 -1.65930235189225 -8.70401952259628
0.0402825645227914 -0.831652038996936 -4.33943736027042
0 0 0
0.0402825645227914 0.831652038996936 4.33943736027042
0.161495976000238 1.65930235189225 8.70401952259628
0.364772484005884 2.47885447851159 13.1202338257239
0.652123873158525 3.28601050601004 17.617459181453
1.02665869693418 4.07613690255669 22.229993608725
1.49296038691012 4.84407863222096 27

Xa Ya anglea
10.2530951925885 -3.04934218244338 -16.5628457602308
10.6683186489426 -2.06615604076629 -10.9608966560158
10.9171199762502 -1.04290879749689 -5.45688704168193
11 0 0
10.9171199762502 1.04290879749689 5.45688704168193
10.6683186489426 2.06615604076629 10.9608966560158
10.2530951925885 3.04934218244338 16.5628457602308
    
```

Figure A4: Exporting port position in MATLAB console

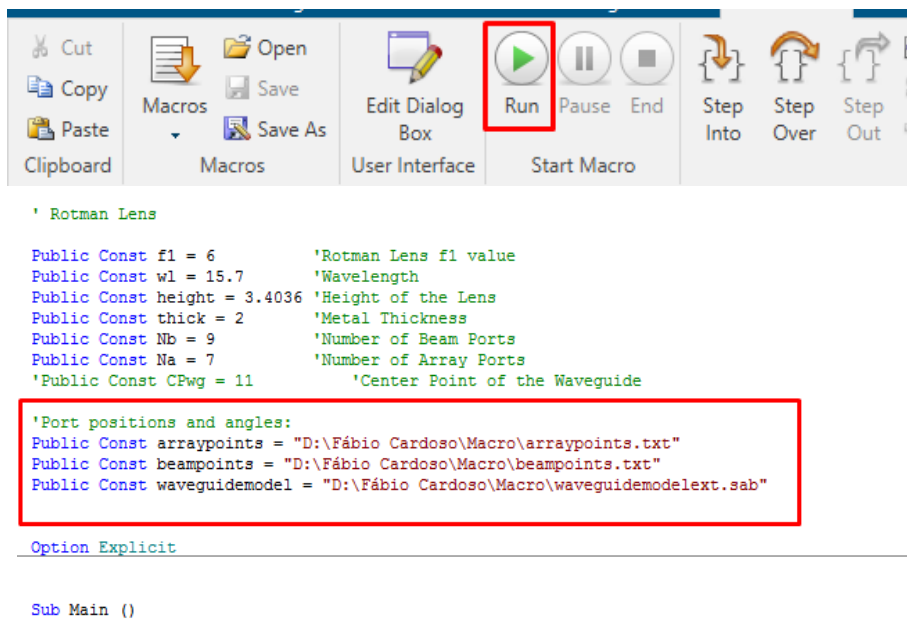


Figure A5: Running the CST macro and importing the generated.txt files

Section 5:

In this Section, we have a visual guide for the user, so he can understand with ease where each parameter is located.

Section 6:

In this Section, some considerations to take into account while using the application, mostly suggestions from other works.

B. Macro CST

In this attachment it is shown the macro developed for this work. The language used is VBA, and the macro can be executed in CST – MICROWAVE STUDIOS.

```
' Rotman Lens

Public Const f1 = 6           'Rotman Lens f1 value
Public Const wl = 15.7       'Wavelength
Public Const height = 3.4036 'Height of the Lens
Public Const thick = 2       'Metal Thickness
Public Const Nb = 9          'Number of Beam Ports
Public Const Na = 7          'Number of Array Ports
Public Const CPwg = 11       'Center Point of the Waveguide

'Port positions and angles:
Public Const arraypoints = "N:\Fábio Cardoso\Macro\arraypoints.txt"
Public Const beampoints = "N:\Fábio Cardoso\Macro\beampoints.txt"
Public Const waveguidemodel = "N:\Fábio Cardoso\Macro\waveguidemodel-ext-short.sab"
Option Explicit
Sub Main ()

    BeginHide
    BuildLens()
    Component.New "Beam Waveguides"
    BuildBeamWaveguides()
    Component.Delete "component1"
    Component.New "Array Waveguides"
    BuildArrayWaveguides()
    Component.Delete "component1"
    EndHide
End Sub

Sub BuildLens()

    With Cylinder
```

```
.Reset  
.Name "Upper Lens"  
.Component "Rotman Lens"  
.Material "PEC"  
.OuterRadius f1*wl/2  
.InnerRadius "0.0"  
.Axis "z"  
.Zrange height/2, height/2+thick  
.Xcenter f1*wl/2  
.Ycenter "0"  
.Segments "0"  
.Create
```

End With

With Cylinder

```
.Reset  
.Name "Bottom Lens"  
.Component "Rotman Lens"  
.Material "PEC"  
.OuterRadius f1*wl/2  
.InnerRadius "0.0"  
.Axis "z"  
.Zrange -height/2-thick, -height/2  
.Xcenter f1*wl/2  
.Ycenter "0"  
.Segments "0"  
.Create
```

End With

With Transform

```
.Reset  
.Name "Rotman Lens"  
.Origin "Free"  
.Center "0", "0", "0"
```

```
.ScaleFactor "1.2", "2", "1"  
.MultipleObjects "False"  
.GroupObjects "False"  
.Repetitions "1"  
.MultipleSelection "False"  
.Transform "Shape", "Scale"  
End WithWith Transform  
.Reset  
.Name "Rotman Lens"  
.Vector -wl/2, "0", "0"  
.UsePickedPoints "False"  
.InvertPickedPoints "False"  
.MultipleObjects "False"  
.GroupObjects "False"  
.Repetitions "1"  
.MultipleSelection "False"  
.Transform "Shape", "Translate"  
End With  
End Sub
```

```
Sub BuildBeamWaveguides()
```

```
Dim textline As String  
Dim Text As Variant  
Dim Dx As Double  
Dim Dy As Double  
Dim angle As Double  
Dim i As Double  
Dim Name As String
```

```
Open beampoints For Input As #1
```

```
i = 1
```

```
Do Until EOF(1)
```

```
Line Input #1, textline
```

```
        Text = Split(textline, "      ")
        Name = "BeamPort-" & i
        Dx = Cdbl(Text(0))*wl
        Dy = Cdbl(Text(1))*wl
        angle = Cdbl(Text(2))
        PlaceBeamWaveguide(Dx, Dy, angle, Name)
        i += 1
    Loop
Close #1

End Sub

Sub PlaceBeamWaveguide(Dx As Double, Dy As Double, angle As Double, Name As
String)With SAT
    .Reset
    .FileName waveguidemodel
    .Id "1"
    .Version "9.0"
    .ScaleToUnit "0"
    .ImportToActiveCoordinateSystem "True"
    .Curves "True"
    .Read
End With

Pick.PickPointFromCoordinates Dx, Dy, "0"
Pick.PickPointFromCoordinates "0", "0", "0"

With Transform
    .Reset
    .Name "component1"
    .Vector Dx, Dy, 0
    .UsePickedPoints "True"
    .InvertPickedPoints "True"
    .MultipleObjects "False"
```



```
.GroupObjects "False"
.Repetitions "1"
.MultipleSelection "False"
.Transform "Shape", "Translate"
End WithWith Transform
.Reset
.Name "component1"
.Origin "Free"
.Center Dx, Dy, "0"
.Angle "0", "0", -angle
.MultipleObjects "False"
.GroupObjects "False"
.Repetitions "1"
.MultipleSelection "False"
.Transform "Shape", "Rotate"
End With

Solid.ChangeComponent "component1:Waveguide", "Beam Waveguides"

Solid.Rename "Beam Waveguides:Waveguide", Name

End SubSub BuildArrayWaveguides()

Dim textline As String
Dim Text As Variant
Dim Dx As Double
Dim Dy As Double
Dim angle As Double
Dim i As Double
Dim Name As String

    Open arraypoints For Input As #1
    i = 1
        Do Until EOF(1)
```

```
        Line Input #1, textline
        Text = Split(textline, "      ")
        Name = "Array-" & i
        Dx = Cdbl(Text(0))*wl
        Dy = Cdbl(Text(1))*wl
        angle = Cdbl(Text(2))
        PlaceArrayWaveguide(Dx, Dy, angle, Name)
        i += 1
    Loop
Close #1

End SubSub PlaceArrayWaveguide(Dx As Double, Dy As Double, angle As Double, Name As
String)With SAT
    .Reset
    .FileName waveguidemodel
    .Id "1"
    .Version "9.0"
    .ScaleToUnit "0"
    .ImportToActiveCoordinateSystem "True"
    .Curves "True"
    .Read
End WithWith Transform
    .Reset
    .Name "component1"
    .Origin "Free"
    .Center "0", "0", "0"
    .Angle "0", "0", angle+180
    .MultipleObjects "False"
    .GroupObjects "False"
    .Repetitions "1"
    .MultipleSelection "False"
    .Transform "Shape", "Rotate"
End With
```

Pick.PickPointFromCoordinates "0", "0", "0"

Pick.PickPointFromCoordinates Dx, Dy, "0" With Transform

.Reset

.Name "component1"

.Vector Dx, Dy, "0"

.UsePickedPoints "True"

.InvertPickedPoints "False"

.MultipleObjects "False"

.GroupObjects "False"

.Repetitions "1"

.MultipleSelection "False"

.Transform "Shape", "Translate"

End WithSolid.ChangeComponent "component1:Waveguide", "Array Waveguides"

Solid.Rename "Array Waveguides:Waveguide", Name

End Sub

C. Submitted Article for EuCAP 2022

Design of a Rotman Lens Operating in the Full K/K_a Band Using Ridge Waveguide Technology

Fábio Cardoso^{1,2}, Sérgio Matos^{1,2}, Jorge Costa^{1,2}, Carlos Fernandes^{2,3}, João Felício^{2,4}, Nelson J. G. Fonseca⁵

¹ Department of Information Science and Technology, University Institute of Lisbon (ISCTE-IUL), Lisbon, Portugal, Fabio_Cardoso@iscte-iul.pt, sergio.matos@iscte-iul.pt

² Instituto de Telecomunicações (IT), Lisbon, Portugal.

³ Department of Electrical and Computer Engineering, Instituto Superior Técnico (IST), University of Lisbon, Lisbon, Portugal

⁴ Centro de Investigação Naval (CINAV), Escola Naval, 1400-203 Almada, Portugal

⁵ European Space Agency, Antenna and Sub-Millimetre Waves Section, Noordwijk, The Netherlands

Abstract— Several services associated with satellite on the move and 5G applications are populating the K and K_a frequency bands. Beam forming networks are crucial components for achieving the necessary beam flexibility and agility of these systems. The Rotman lens is being widely investigated as a cost-effective solution for overcoming the main limitations of other types of beam forming networks, namely bandwidth, complexity, and size. One of the main design challenges is obtaining broadband transitions for the array and beam ports. In this work, we used a standard K/K_a double ridge (WRD180) for interfacing with the Rotman Lens. The main motivation for this choice is the wide bandwidth, compatible with the K/K_a satcom frequency bands, and the use of air/vacuum propagation medium in the parallel plate waveguide section to avoid dielectric losses associated with microstrip implementations. We present a design capable of fully exploiting the ridge waveguide bandwidth with wide beam scanning, outperforming previous works. The presented design consists of a 13×7 Rotman Lens with a scanning range of ±50 degrees operating between 16 and 40 GHz, validated through full-wave simulations.

Index Terms—5G, Satellite on the move, Beam forming networks, Rotman Lens, Double Ridge Waveguide, K/K_a Band

I. INTRODUCTION

The demand for ubiquitous broadband internet access is pushing forward the development of new mobile terrestrial and space communication infrastructures. K and K_a frequency bands are expected to become a common place in a near future of 5G and satellite communications [1]. There is an intense research effort on the development of broadband (multi)beam antennas [2], [3]. The design of the corresponding beam forming networks (BFNs) is particularly challenging for millimetre-waves, as they become more inefficient and complex with the increase of the operation frequency and aperture size relative to the wavelength in order to compensate for higher propagation losses. For these reasons, quasi-optical beamforming solutions are considered well suited for higher frequencies [4]. In particular, the Rotman lens (RL) [5], as a true time delay BFN, offers a combination of broadband operation with low-cost, compactness and wide-angle beam steering. Continuous improvements and variation on this classic topic are still being put forward [6]-[10]. This work

presents a Rotman Lens design with wide-angle (±50°) and ultra-wide band (16-40 GHz) using standard double ridgewaveguides (WRD180) as array and beam ports. In fact, the combination of the large operation bandwidth of ridge waveguides and of the Rotman lens has been previously reported [6], [9]-[11]. Specifically, an exhaustive comparison between different feeding port designs was provided in [10], which confirmed the superior performance of ridged waveguide designs. In [6], ultrawideband was achieved but only for a limited scanning range and small number of array and beam ports (5×5). The impact on the operating bandwidth of the transitions between the array and beam ports to the central parallel plate waveguide (PPW) was investigated in [11], indicating a careful design is required to achieve an ultrawideband response with waveguide ports, even when ridged waveguides are implemented.

In this paper, a novel transition design is proposed which demonstrates superior performance compared to previously reported ones. Specifically, the sidewalls of the ridged waveguides are not connected as in previously reported designs. Instead, a longitudinal corrugation is implemented between each feeding ports, which has a positive impact on the return loss and port-to-port coupling at the expense of a moderate increase in the distance between adjacent ports. A standard WRD180 double ridge waveguide (18-40 GHz) is used as the input and output ports of a 13×7 Rotman lens with a scanning range of ±50 degrees. Bézier curves is applied in the design of the Rotman lens transmission lines (TLs). This method provides smooth curvature, which is particularly important when aiming for ultrawideband operation, as is the case in this work. The results were validated by full-wave simulations using CST microwave studio [12]. The return losses of the presented design are better than 10 dB even beyond the K/K_a bands of interest for satcom applications (16-40 GHz). The proposed design outperforms previous works when comparing return loss, wide angle scanning and bandwidth. The work paves the way for a future experimental validation that is being planned.

II. ROTMAN LENSES DESIGN

A. Geometry

The general design rules of a RL are well establish [13], which are based on Geometrical Optics for the definition of the paths from the Beam Ports (BPs), through the Array Ports (APs) and ending at the Radiating Elements (RE) (Figure 1). However, these initial values need to be adjusted considering the real structure of the beam and array ports (in our case standard ridges WRD180) and corresponding transitions to the PPW. The design parameters are shown in Table 1. These values followed from an iterative optimization using preliminary full-wave tests. We adopt a 13×7 configuration with a ± 50 degrees scanning range, which is a representative example of a RL design for 5G and satellite-on-the-move (SOTM) applications. We limit the number of ports to keep the associated computational effort manageable, which is required for full-wave optimizations. A practical design may be adapted in size to meet given requirements. The focal length f_1 was kept as low as possible ensuring low reflections and good illuminations of the array ports according to full-wave results. The value of β , that controls the shape of the focal arc, was adjusted to minimize the coupling between adjacent ports. The profile of the focal arc and inner lens contour are shown in Figure 2.

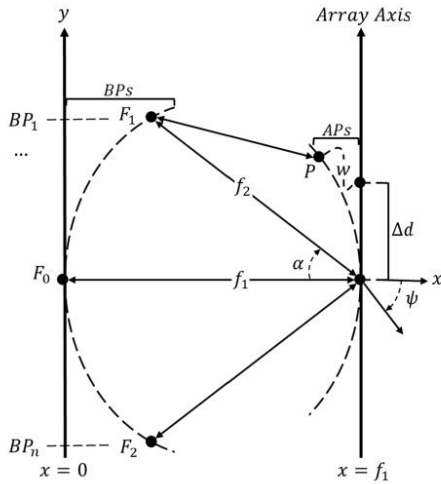


Figure 1. Rotman lens schematics [13].

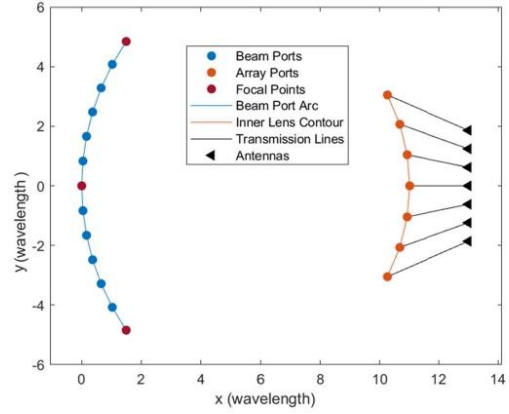


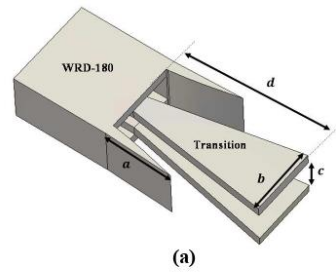
Figure 2. Profile of the designed Rotman lens .

Table 1 – Design parameter of the Rotman Lens.

Variable	Value
Number of input ports	13
Number of output ports	7
Focal angle, α	$\pm 27^\circ$
Focal ratio, $\beta = f_2/f_1$	0.97
Maximum beam angle, ψ_{\max}	$\pm 50^\circ$
Focal length, f_1 (mm)	137
Array element spacing, Δd (mm)	9.7

B. Double Ridge to PPW Transition

A proper design of a transition is required to ensure a wideband behaviour of the lens. The design proposed in [10] was adapted and optimized to operate between 16 and 40 GHz. The final dimensions are shown in Figure 3, which also contains a representation of the positioning of these transitions along the focal arc, illustrating the longitudinal corrugation introduced between adjacent ports (Figure 2b).



(a)

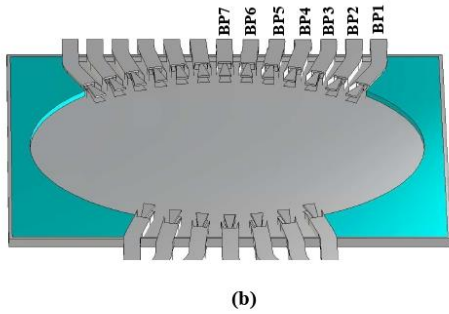


Figure 3. (a) Geometry of the design Ridge to PPW transitions with $a = 7 \text{ mm}$, $b = 6.8 \text{ mm}$, $c = 3.4 \text{ mm}$, $d = 14.9 \text{ mm}$. (b) Transitions in the Rotman lens.

C. Assembling the Rotman lens

After positioning all the lens components in the previously calculated locations, the lens is closed. The PPW takes a rectangular shape filled with absorbing material (ECCOSORB NA 77) on the sides so that reflections due to spillover are minimized. In fact, absorbing material was also included originally between each feeding ports within the rectangular cavity. It was found that removing them would not affect notably the performance, thus simplifying the design and assembly. This also introduces new design parameters with the length of these longitudinal corrugations, which may be further investigated in the future. The remaining absorbing material on the sides of the cavity can be removed as well, by adding new ports (including dummy ports) which would allow achieving an all-metal design. Finally, the TLs, designed using Bézier curves, are added, completing the RL beamformer. Figure 4 shows the final design of the lens.

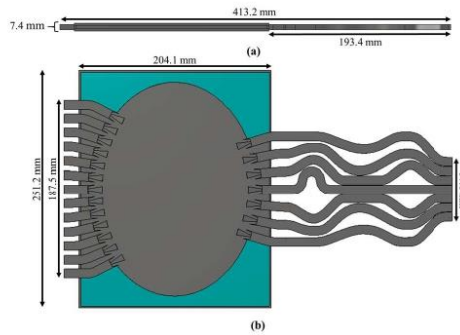


Figure 4. 3D Model representation [CST]: (a) side view, (b) top view.

III. NUMERICAL RESULTS AND DISCUSSION

This section shows the full-wave simulation results of the model presented in Figure 4. The model was simulated from

16 to 40 GHz using the FDTD solver of CST Microwave Studio. In Figure 5 it is shown that all the scattering parameters between the beam ports are well below -10 dB over the entire analysed band.

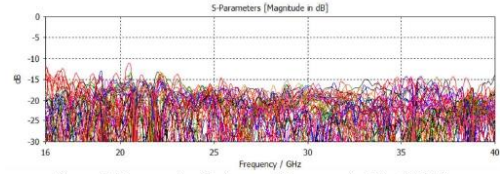


Figure 5. S-parameters between all beam ports 16 to 40 GHz.

The field amplitude and phase representation inside the lens is shown in Figure 6 for different beam ports at 30 GHz. This representation highlights the role of the cavities between the arrays ports on reducing reflections back to the beam ports. As expected, a significant spill over is observed due to the small size of the array contour. This may be mitigated adding more array ports; however, it would increase the numerical complexity of the analysis. The presented design is sufficient for showing the broadband potential of this approach.

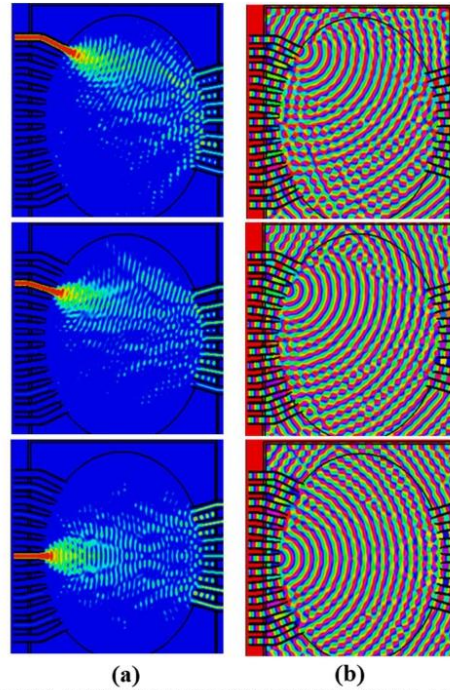
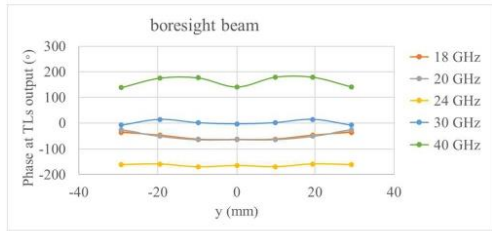


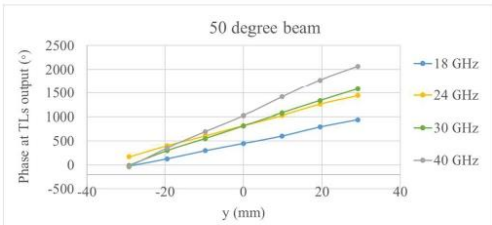
Figure 6. Amplitude (a) and phase (b) field distribution inside RL for 30 GHz for three different beam port excitations.

Figure 7 shows the phase variation at the output of the TLs for two beam positions, the central one and the most scanned

one, confirming the stable design of the complete beamformer over the analysed frequency range. In Table 2 the beam direction and corresponding phase errors are also presented. The corresponding array factors for port 1, 3 and 7 for 18 and 30 GHz are represented in Figure 8. A good agreement of the full-wave results with the reference case of ideal linear phase variation and constant amplitude is obtained. Finally, in Table 3 the presented design is compared with other broadband RL designs in terms of lens size, TL technology, scanning range, frequency range and 10 dB return loss bandwidth. This comparison clearly highlights the benefits of presented design.



(a)



(b)

Figure 7. Phase at the output ports of the TLs (each dot corresponds to a different TL) considering multiple frequencies for the central port (a) and most scanned one (b).

Table 2 –Beam direction and average phase error for sequential beam port excitation (see Figure 3b), at 18 GHz, 30 GHz, 40 GHz.

BP (#)	18 GHZ		30 GHZ		40 GHZ	
	Ψ (°)	Average Error(°)	Ψ (°)	Average Error(°)	Ψ (°)	Average Error(°)
1	50.6	7.1	48.9	12.0	49.0	19.9
2	40.2	9.8	39.9	10.0	39.1	19.7
3	30.8	5.6	30.7	11.2	30.1	13.6
4	23.0	9.5	22.6	15.0	22.0	19.7
5	14.9	9.8	14.0	12.7	14.3	28.0
6	7.7	9.3	7.5	15.7	7.0	20.8
7	0.0	10.2	0.0	7.0	0.0	18.5

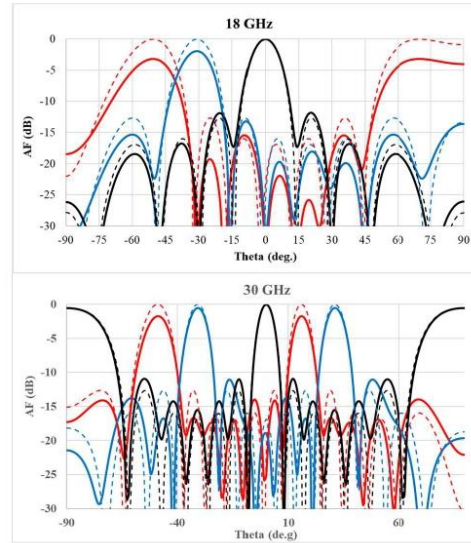


Figure 8. Array factors for ports 1, 3 and 7 at 18 GHz and 30 GHz. Comparison of the full-wave simulations (solid lines) with the case of ideal linear phase variations and constant amplitude (dashed lines).

Table 3 – Comparing different broadband Rotman lens designs.

	Size	Tech.	Scan	Freq. (GHz)	10 dB Bandwidth
[6]	5×5	Ridge	$\pm 30^\circ$	6-18	100%
[8]	18×16	Microstrip + PMU	$\pm 30^\circ$ RL $\pm 60^\circ$ RL+PMU	20-25	23%
[10]	13×11	Ridge	$\pm 15^\circ$	37-43	15%
This work	13×7	Ridge	$\pm 50^\circ$	16-40	86%

IV. CONCLUSION

This work presented a Rotman lens design with ultrawide band operation and wide angular scanning range. The bandwidth potential of WRD180 double ridge waveguides was fully exploited thanks to a novel design of transitions between the beam/array ports and the PPW section. This work confirms the potential of ridge waveguide technology for millimeter wave applications. Future works will include investigations on the design of the proposed longitudinal corrugations, as well as experimental validation.

ACKNOWLEDGMENT

This work was partially supported by Fundação para a Ciência e Tecnologia (FCT) under projects PTDC/EEI-TEL/30323/2017 (“ADAM3D”) and UIDB/50008/2020

REFERENCES

- [1] O. Kodheli *et al.*, "Satellite Communications in the New Space Era: A Survey and Future Challenges," *IEEE Communications Surveys & Tutorials*, vol. 23, no. 1, pp. 70-109, Firstquarter 2021
- [2] S. Ghosh and D. Sen, "An Inclusive Survey on Array Antenna Design for Millimeter-Wave Communications," *IEEE Access*, vol. 7, pp. 83137-83161, 2019.
- [3] Y. J. Guo, M. Ansari and N. J. G. Fonseca, "Circuit Type Multiple Beamforming Networks for Antenna Arrays in 5G and 6G Terrestrial and Non-Terrestrial Networks," *IEEE J. Microwaves*, vol. 1, no. 3, pp. 704-722, July 2021.
- [4] Y. J. Guo, M. Ansari, R. W. Ziolkowski and N. J. G. Fonseca, "Quasi-Optical Multi-Beam Antenna Technologies for B5G and 6G mmWave and THz Networks: A Review," *IEEE Open J. Antennas Propag.*, vol. 2, pp. 807-830, 2021.
- [5] W. Rotman and R. F. Tumer, "Wide-Angle Microwave Lens for Line Source Applications," *IEEE Trans. Antennas Propag.*, vol. 11, no. 6, pp. 623-632, 1963.
- [6] K. V. Hoel, S. Kristoffersen, N. Jastram and D. S. Filipovic, "3D printed Rotman lens," 2017 47th European Microw. Conf. (EuMC), 2017, pp. 125-128.
- [7] N. J. G. Fonseca, "A Focal Curve Design Method for Rotman Lenses With Wider Angular Scanning Range," *IEEE Antennas Wirel. Propag. Lett.*, vol. 16, pp. 54-57, 2017
- [8] E. Tolin, O. Litschke, S. Bruni and F. Vipiana, "Compact Extended Scan Range Antenna Array Based on Rotman Lens," in *IEEE Trans. Antennas Propag.*, vol. 67, no. 12, pp. 7356-7367, Dec. 2019.
- [9] S. Gomanne, *et al.*, "Comparative study of waveguide Rotman lens designs for Q/V band applications," 40th ESA Antenna Workshop, Noordwijk, The Netherlands, Oct. 2019.
- [10] S. Gomanne, *et al.*, "Rotman Lenses with Ridged Waveguides in Q-Band," 2020 14th European Conf. Antennas Propag. (EuCAP), 2020, pp. 1-5.
- [11] P. Knott, "Design of a ridged waveguide feed network for a wideband Rotman lens antenna array," 2008 *IEEE Radar Conf.*, 2008, pp. 1-4.
- [12] Dassault Systèmes, CST studio suite: electromagnetic field simulation software, <https://www.3ds.com/products-services/simulia/products/cst-studio-suite/> [online 13 October 2021].
- [13] R. C. Hansen, "Design trades for Rotman lenses," *IEEE Trans. Antennas Propag.*, vol. 39, no. 4, pp. 464-472, Apr. 1991.